

# **Annealing effects on Accumulative Roll Bonded Aluminium laminates of different purities**

Bhupendra Sharma

A Dissertation Submitted to  
Indian Institute of Technology Hyderabad  
In Partial Fulfillment of the Requirements for  
The Degree of Master of Technology (M.Tech.)



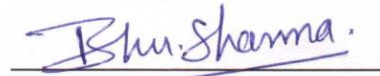
भारतीय प्रौद्योगिकी संस्थान हैदराबाद  
Indian Institute of Technology Hyderabad

Department of Materials Science and Engineering

1<sup>st</sup> July, 2013

## Declaration

I declare that this written submission represents my ideas in my own words, and where others' ideas or words have been included, I have adequately cited and referenced the original sources. I also declare that I have adhered to all principles of academic honesty and integrity and have not misrepresented or fabricated or falsified any idea/data/fact/source in my submission. I understand that any violation of the above will be a cause for disciplinary action by the Institute and can also evoke penal action from the sources that have thus not been properly cited, or from whom proper permission has not been taken when needed.



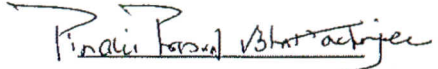
(Signature)

(Bhupendra Sharma)

(Roll No:-MS11M01)

# Approval Sheet

This thesis entitled – Annealing effects on Accumulative roll bonded Aluminium laminates of different purities by Mr. Bhupendra Sharma is approved for the degree of Master of Technology (M.Tech) from IIT Hyderabad.



Dr. Pinaki Prasad Bhattacharjee

(Department of Materials Science and Engineering)

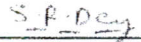
Examiner



Dr. Bharat Bhooshan Panigrahi

(Department of Materials Science and Engineering)

Examiner



Dr. Suhash Ranjan Dey

(Department of Materials Science and Engineering)

Adviser



Dr. Manish Niranjana

(Department of Physics)

Chairman

## Acknowledgements

This research work would not have been possible without the support and guidance of many peoples.

First of all, I would like to express my sincere gratitude to my guide, **Dr. Suhash Ranjan Dey**, for his guidance, patience, understanding, encouragement and most importantly, support over the years during my M.Tech studies at IIT Hyderabad. I would like to express my thanks to him for encouraging me to do my huge project work with in respective deadlines without any pressure. He always helped me for writing and correcting my thesis and various proposals and due to his very much support I have got a Ph.D. position.

Once again thanks to my guide and our respected director **Prof. Uday B. Desai** and head of materials science department **Dr. Pinaki Prasad Bhattacharjee** for their support to provide project facilities within the IIT Hyderabad campus.

I would like to convey my grateful thanks to Ph.D. research scholars Mr. Dan Sathiaraj, Mr. Basanth Kumar K, Miss Sushmita Chaudhari for their support and guidance during my research work to perform tests and characterization.

I would like to acknowledge all Ph.D. research scholars and my M.Tech classmates and IIT Hyderabad Friends to be a part of my life and help me during my M.Tech study.

Finally; I would like to express my love and gratitude to my beloved family; my father Mr. Prahlad Sharma and my mother Santosh Sharma and my sisters Dr. Varsha Sharma and Poonam Sharma to be always with me and became my back bone whenever I felt any problem during my study. There love never realized me alone and discouraged during my study.

Bhupendra Sharma



Dedicated to

**My Family Members:**

**My Father: Mr. Prahlad Sharma**

**My Mother: Mrs. Santosh Sharma**

**My Sisters: Dr. Varsha Sharma and Poonam Sharma**

Because they believe in me whatever I am doing is for my future and that's why every time their trust and support motivate me to work hard and honestly

## Abstract

Accumulative roll-bonding (ARB) is a severe plastic deformation technique which is used for ultrafine grains development in bulk laminates. Composite laminates of dissimilar materials can also be bonded through ARB. In the present work different purity aluminium laminates are roll bonded and annealed at different temperatures to study their static recrystallization behavior. Aluminium laminates of commercial pure 99.5 weight % (henceforth will be called as “A”) and ultra-high pure 99.999 weight % (will be called as “C”) after annealed at 500°C for 1 hour and roll bonded up to 10 rolling cycles, are as-received. These are heat treated for 30 mins in salt bath furnace from 150°C to 450°C with 25°C temperature intervals followed by water quenching and its further hardness, microstructural characterization and crystallographic texture studies are carried out on them. Vickers Micro-Hardness studies explained hardness profiles with different number of rolling cycles and annealing temperatures. Simultaneous studies using scanning electron microscopy (SEM)-electron backscattered diffraction (EBSD) mappings, their recovery, recrystallization and grain growth phenomena could be analyzed. For as-received roll bonded samples, it is observed that with increasing number of rolling cycles hardness decreased (dynamic recovery and recrystallization) and then increased (deformation of the recrystallized grains) during ARB processing itself. But for the heat treated samples at all the temperatures, hardness values for each rolled cycles is decreased from their roll bonded values (due to recovery, static recrystallization and grain coarsening). The SEM-EBSD maps of rolled ARB specimens showed discontinuous dynamic recrystallization in ultra-high pure aluminium (C) layer and dynamic continuous recovery/recrystallization in commercially pure aluminium (A) layer, which ultimately developed into ultrafine grained microstructure by 10 cycles of ARB. Static recrystallization and grain coarsening is noticed through SEM-EBSD mapping after heat treatment of these ARB specimens, which first changed the ultrafine grained ARB microstructure into coarse long cellular-type microstructure and then coarsened into large equiaxed microstructure. The SEM-EBSD orientation maps also provided their crystallographic texture evolution details with each cycles and its heat treatments. In ARB specimens (AC-1 to AC-10) Cube and shear Cube texture components are majorly noted in C layer with Copper, S, Shear Copper and Shear S are found in A layer. The shear components might be generated from the friction between the rolls and the specimen surface. Whereas, annealing of all the ARB specimens mostly produced coarse grain Cube texture mainly through static recrystallization and grain coarsening.

## Nomenclature

ARB	-	Accumulative roll-bonding
UFG	-	Ultrafine grained
SPD	-	Severe Plastic Deformation
ECAP	-	Equal channel angular pressing
HPT	-	high pressure torsion
SEM	-	Scanning Electron Microscope
EBS	-	Electron Back-scattered diffraction
PF	-	Pole Figure
IPF	-	Inverse Pole Figure
ND	-	Normal direction
TD	-	Transverse direction
RD	-	Rolling direction
ODF	-	Orientation distribution function
SRX	-	Static Recrystallization
DRV	-	Dynamic Recovery
CDRX	-	Continuous dynamic recrystallization
SFE	-	Stacking fault energy
YS	-	Yield strength
FCC	-	face centered cubic
GNBs	-	Geometrically necessary boundaries
IDBs	-	Incidental dislocation boundaries
BHT	-	Before Heat Treatment

# Contents

Declaration.....	
<b>Error! Bookmark not defined.</b>	
Approval Sheet.....	<b>Error!</b>
<b>Bookmark not defined.</b>	
Acknowledgements.....	iv
Dedication.....	v
Abstract.....	vi
<b>Nomenclature .....</b>	<b>.vii</b>
<b>1 Introduction .....</b>	<b>Error! Bookmark not defined.</b>
1.1 Ultra fine Grains (Nano structured grains).....	1
1.2 Severe Plastic Deformation (SPD).....	2
1.2.1 Accumulative Roll Bonding (ARB).....	3
<b>2 Literature Survey.....</b>	<b>6</b>
2.1 Microstructure Evolution in FCC metals during ARB.....	6
2.2 Deformation Texture in FCC materials .....	8
2.3 Recrystallization Texture of FCC metals.....	10
2.4 Why Aluminium and it's alloys?.....	13
<b>3 Objectives of the present work.....</b>	<b>15</b>
<b>4 Experimental Process .....</b>	<b>16</b>
4.1 As-received Sample and its Cutting.....	16
4.2 Annealing.....	16
4.3 Hot Mounting.....	16
4.4 Grinding and Polishing.....	17
4.5 Optical Microscope.....	17
4.6 Micro Hardness Test.....	17
4.7 Electro Polishing.....	17
4.8 Electron Backscattered Diffraction (EBSD) attached with SEM.....	18
<b>5 Results and Discussions.....</b>	<b>19</b>
5.1 Initial specimen.....	19
5.2 ARB specimen from AC-1 to AC-10.....	20

5.3 Texture evolution from AC-1 to AC-10.....	23
5.4 Annealing Effects from AC-1 to AC-10.....	24
5.5 Texture Evolution from Annealing (AC-1 to AC-10).....	36
<b>6 Summary.....</b>	<b>37</b>
<b>7 Future Works.....</b>	<b>39</b>
<b>References.....</b>	<b>40</b>
<b>Appendix.....</b>	<b>44</b>

# Chapter 1

## Introduction

### 1.1 Ultra-fine grains

Mechanical properties of polycrystalline metals and alloys are highly dependent on the average grain size present in their microstructure. Since, plastic deformation in the material is carried through dislocation movements, and it is fact that the materials can be strengthened by pinning of its dislocation movements. Therefore, with increasing grain boundaries i.e. smaller grains free dislocation movements can be hindered. Hall (1951) and Petch (1953) suggest a pioneer work that with decreasing grain size yield strength increases. Therefore, metals and alloys with grains of ultra-fine range (from 100- 1000 nm ) are of special interest because they provide excellent mechanical and physical properties. Fine grained materials have several advantages for industrial applications due to its superplastic characteristic, improved formability at elevated temperature, high tensile strength and reasonably good fracture toughness. Especially low strength high purity, commercially pure materials and low alloyed materials can be dramatically strengthened through this way (ultra fine microstructuring).

According to Hall-Petch equation the yield stress of polycrystalline metals and grain diameter is related as:

$$\sigma_y = \sigma_0 + kd^{-1/2}$$

Where: k is constant

$\sigma_0$  is friction stress

$\sigma_y$  is yield stress

d is grain diameter

Ultrafine grains are the Nano sized grains of the range ~100- 1000 nm which is the upper limit of Nano crystalline(NC) or Nano structured materials having grain size ~1- 100 nm.

There are two approaches to develop UFG materials:

- (i) Bottom-Up approach - which include electro deposition [1], inert gas condensation [2], High energy ball milling [3], chemical and physical deposition [4], and sintering [5] etc. These approaches involve assembling UFG materials from Nano particles, atom, ion or molecules. But the limitations of these methods are porosity and trapped gases which are the main reason of failures of materials.
- (ii) Top-Down approach - which includes various severe plastic deformation techniques such as ECAP, ARB and HPT. These approaches are based on development of UFG by the processing of coarse grained materials to develop fine grained materials.

These approaches have many advantages over Bottom-Up approaches, by generation of negligible porosity and less contamination. However, these methods are not limitation free and have many limitations such as bulk production, variable properties due to degree of instability in microstructure) [6-8].

## **1.2 Severe Plastic Deformation**

Severe plastic deformation (SPD) can be defined as a metal forming process in which huge plastic strain is introduced in metal below the recrystallization temperature to obtain ultra-fine grained (average grain size less than 1  $\mu\text{m}$ ) metals. Though plastic deformation processes have been used for many decades, but in this modern era its upgraded version (SPD techniques) is developed in which the shape and dimension of the work piece doesn't change after processing hence imparting large strain, whilst avoiding any contamination that may be introduced in other techniques. Older techniques such as extrusion, rolling, forging are some examples in which the dimension of the output sample doesn't remain same as input material. The objective behind severe plastic deformation is to produce high strength at low temperature in lightweight metal parts without adding alloy elements and without affecting environmental harmony. The significant feature of SPD processes is that even after processing of the material it's dimension doesn't change. In this area many researchers developed various SPD techniques such as equal channel angular pressing (ECAP) [9,10], high pressure torsion (HPT) [10,11], accumulative roll bonding (ARB) [12-15], cyclic extrusion compression (CEC) [16], multi axial forging (MAF) [17], constrained groove pressing (CGP) [18] severe torsion straining (STS) [19],etc. Among these techniques the most investigated and developed techniques are ECAP, ARB and HPT.

These SPD methods may be classified on the basis of their strain paths and this huge strain can be achieved by various methods [20]:

- (i) Continuous strain without change of strain path: compression, extrusion, HPT
- (ii) Accumulated strain without change of strain path: rolling, drawing, ECAP (route A)
- (iii) Accumulated strain with reversal of strain path: cyclic-extrusion compression (CEC), ECAP (route C)
- (iv) Accumulated strain with variable strain path: swaging, ECAP ( route B & D), Accumulative roll bonding

A brief introduction of ARB technique is following:

### 1.2.1 Accumulative roll bonding (ARB)

Accumulative roll bonding is an intense plastic deformation process. ARB was first introduced by Saito et al in 1998 [21]. In ARB process, two sheets are brushed on one side each, to minimize any oxide layer and roughen the surface. These are placed together and bonded together by rolling with thickness reduction up to 50 percent. As cold welding takes place during rolling a new bonded sheet is produced. This output rolled material is cut in the transverse direction into two parts, wire brushed and stacked together and roll bonded again. Same process can be repeated many times. The achieved strain is unlimited in this process because repetition times are endless in principal.

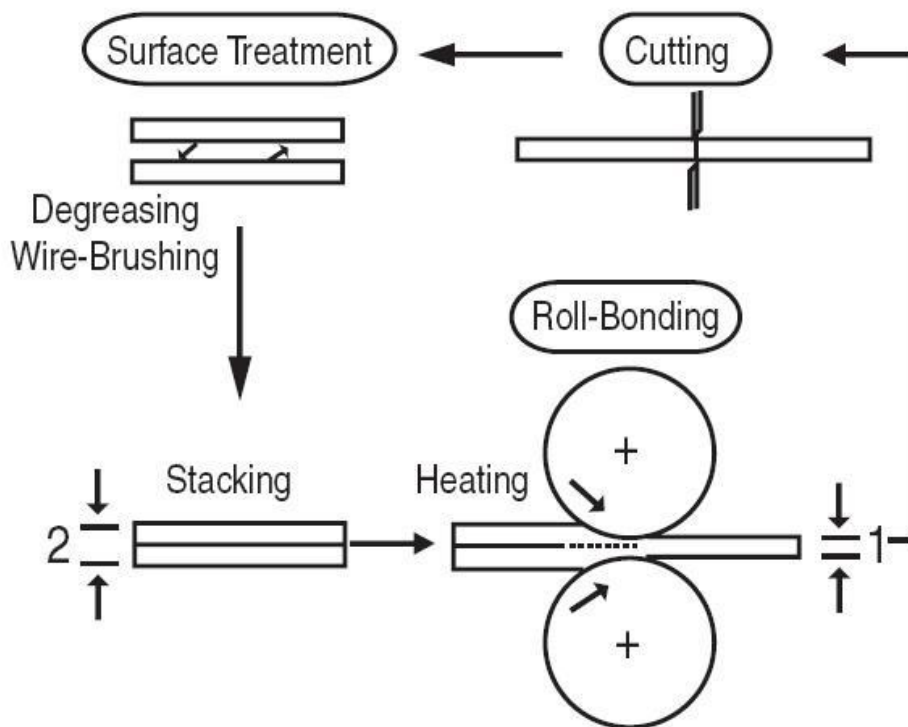




**Figure 1: Schematic representation of ARB process [21].**

However, to reduce the rolling force and to achieve good bonding, the stacked sheets can be heated below the recrystallization temperature of material and roll-bonded simultaneously. A major advantage of ARB is the capacity to produce multilayered sheet composites containing alternative layers of two or more dissimilar metals. Moreover, as it is a continuous process and therefore, can be incorporated for large scale production in industries. Herewith, it can be easily performed by conventional rolling process and therefore, it is mostly appropriate for practical applications. In this process metal sheet deforms in the rolling direction. Its principal limitations are through-thickness non-uniformity of microstructure and edge cracking during rolling to very large strains. Additional work is also needed to maintain acceptable levels of ductility in ARB-processed metals.

After each cycle the number of stacked layer increases according to power law equation [equation-1] and the thickness of each layer can be calculated by equation-2. Thus number of bonded boundaries can be calculated by equation-3.

$$n = 2^N \quad \text{[equation-1]}$$

$$t = t_0 / 2^N \quad \text{[equation-2]}$$

$$b = 2^N - 1 \quad \text{[equation-3]}$$

Where:

$n$  = number of layers after ARB processing

$N$  = number of ARB cycles

$t_0$  = initial thickness of the sheet

$t$  = final thickness of individual layer after ARB processing

$b$  = number of bonded boundaries

Therefore, total reduction in thickness of each layer, after  $N$  number of cycles can be calculated by equation-4.

$$t_{\text{total}} = 1 - t / t_0 = 1 - 1 / 2^N \quad \text{[equation-4]}$$

If the initial metal sheet thickness is 1 mm, after 10 ARB cycles with 50% thickness reduction in each pass, the number of developed layer in sheet material will be 1024 and thickness of individual layer will be nearly about 1 $\mu$ m. Assuming Von Mises yield criterion and plain strain conditions, the total equivalent strain after  $N$  cycles can be calculated by equation-5.

$$\epsilon_{\text{total}} = \{2/\sqrt{3} \cdot \ln (1/2)\} \cdot N = 0.80 \cdot N \quad \text{[equation-5]}$$

Using these equations, the graphs can be drawn between number of ARB cycles with number of developed layers after ARB process, layer thickness, total thickness reduction in percentage and equivalent strain. These graphs are shown below:

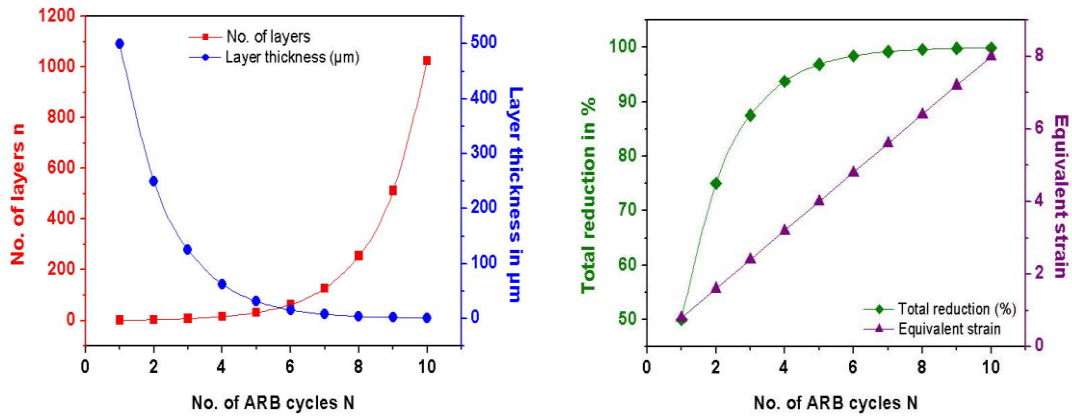


**Figure 2: Geometrical changes for 1mm thick ARB processed sheet by thickness reduction of 50% [22].**

ARB has been used extensively by many researchers and successfully implemented to produces ultrafine grained materials such as Al alloys [23-25], Cu-Ag alloy [26], Zr alloy [27], IF steel [28,29], Ni alloy [30], and multilayered combinations such as Zr/Cu [31], Al/Cu [32], Cu/Co/P [33] and Al-Li [34].

# Chapter 2

## Literature Survey

### 2.1 Microstructural evolution in FCC metals during ARB:

In the rolling process the grains are strongly elongated in the rolling direction and grain size reaches a sub micrometer scale, ranging from 100 nm to 1000 nm. As per Humphreys and Harterly [35], two modes of deformation in metals are slip and twinning, both of these modes are highly dependent on the stacking fault energy (SFE) of the material. Since dislocations readily dissociate in low stacking fault energy (SFE) cubic metals e.g. Cu alloys, thus twinning readily occurs for these types of materials, whereas Slip mode occurs in high SFE cubic materials. The principal slip system for FCC metals is  $\{111\} \langle 110 \rangle$  which are the most closely dense packed planes and directions, respectively. However, grain refinement mechanisms during the ARB process are still not completely understood, but some reports suggest grain subdivision and continuous recrystallization are the basic mechanism for grain refinement due to large strain.

Conventional dislocation theory [36, 37] suggests that during deformation, dislocation density increases continuously and large dislocation density introduced in the material, which results in the intra-granular structure consisting of cells with thick cell walls and low angle misorientation. With increase in strain, the thickness of the cell walls decreases and grain boundaries with large misorientation developed. Consequently, ultrafine grains are formed.

Cells and Sub grains formation: Initially, at low strains, the dislocations are randomly distributed and form dislocation tangles. These dislocations mutually rearrange and form cells. Cells are separated by dense dislocation walls, micro bands, and lamellar boundaries and normally have low angle ( $< 2^\circ$ ) misorientation with each other. For cold rolled aluminum [38], a cellular structure is shown in figure-3. With increase in strain or at higher deformation temperature, cell wall becomes sharpened and cell interior have a low dislocation density, which is called sub grain structure.

Eventually, microstructure evolves into a lamellar structure sandwiching in cells or sub grains, and subdivided into high and low angle grain boundaries. With increasing strain, grain misorientation increases, therefore number of high angle grain boundaries increases [39].

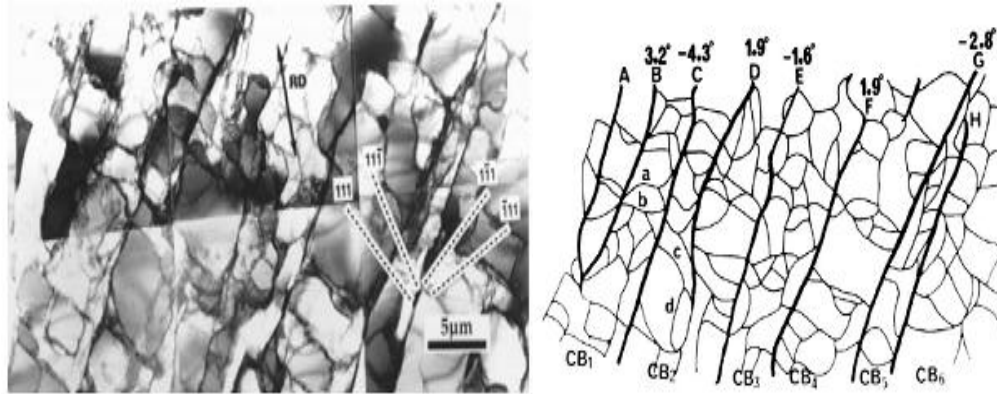


**Figure 3: (a) TEM image of cell block structure in 10% cold rolled (true-strain 0.1) highly pure Al viewed from longitudinal plane, where RD is rolling direction. (b) Cell and cell blocks of same area, misorientation angle between adjacent cell blocks. Cell block boundaries are marked as A, B, C, etc. and cell boundaries are marked as a, b, c, d [40].**

Another theory regarding grain refinement is based on recrystallization mechanism. Humphery and Hatherly [41] suggest that development of ultra-fine grains in severe plastic deformation process is due to continuous recrystallization rather than the conventional discontinuous recrystallization. In the discontinuous recrystallization UFG can be developed by imposing strain and subsequently by annealing [41]. At large strains the HAGBs come closer and they are separated by sub-grains. Once the separation reached up to the sub-grains size, HAGBs becomes immobile. Consequently, equiaxed ultra-fine grains develop. However, usually continuous recrystallization occurs due to annealing after severe plastic deformation or due to strong impingement of grain boundaries by second phase particles. Thus, in the continuous recrystallization mechanism microstructural development occurs without movement of HAGBs [42]. More detailed descriptions from literature on strengthening mechanism, recovery and recrystallization are given in Appendix 1.

## 2.2 Deformation Texture in FCC materials:

The nature of slip in face-centered metals and alloys is strongly affected by the stacking fault energy (SFE) [55], more correctly the specific SFE ( $\gamma/Gb$ ) [56] which is related to the partial dislocations in a dissociated perfect dislocation.

Texture is an important feature for controlling the properties of the ARB-processed sheets, because the ARB process basically fabricates sheet materials [54]. The rolling texture consists of two ‘families’ of orientations, called respectively,  $\alpha$ - and the  $\beta$ - fibre. These fibres form a tube or line through the Euler space [51].

$\alpha$ -fibre: ‘Goss’ (G:  $\{011\} \langle 100 \rangle$ )  $\longrightarrow$  ‘Brass’ (B : $\{011\} \langle 211 \rangle$ )  
 $\beta$ - fibre: ‘Brass’ (B : $\{011\} \langle 211 \rangle$ )  $\longrightarrow$  ‘S’ (S : $\{123\} \langle 634 \rangle$ )  $\longrightarrow$  ‘Copper’  
 (Cu : $\{112\} \langle 111 \rangle$ )

Moreover, during rolling the fcc rolling texture develops which can be further classified according to SFE of the material. Generally, for high and medium stacking fault energy materials like aluminium (SFE: 166 mJ/m<sup>2</sup>) and Copper (SFE: 78 mJ/m<sup>2</sup>), mainly “copper texture” develops. Whereas, for low stacking fault energy materials, like Cu-30 wt% Zn (SFE: 20 mJ/m<sup>2</sup>) and Ag (SFE: 22 mJ/m<sup>2</sup>), the brass texture develops.

Following figure-4 and table-1 represents the rolling texture of fcc metals in Euler space of ( $\Phi_1 = 90^\circ, \Phi = 90^\circ, \Phi_2 = 90^\circ$ ).

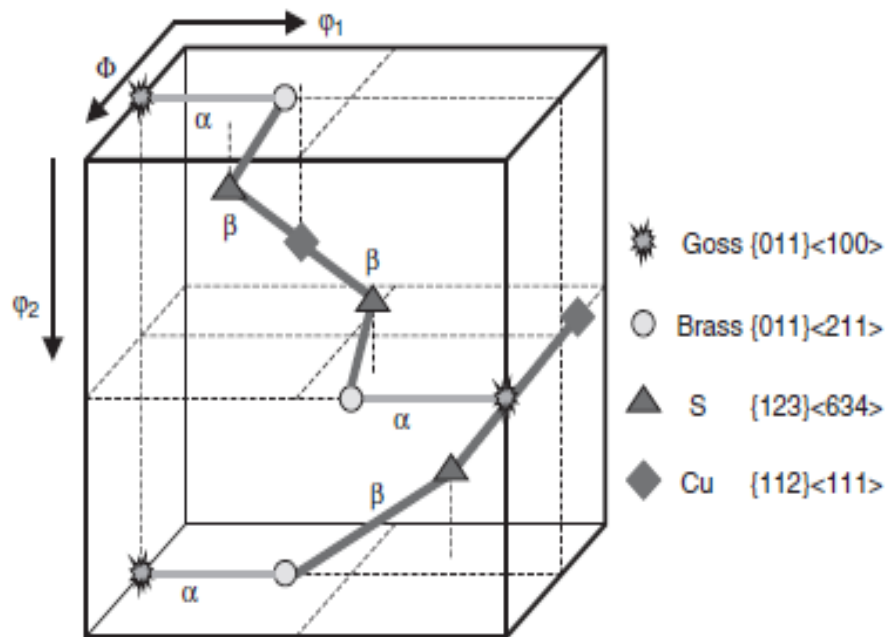


Figure 4: Schematic representation of the cold rolling texture of FCC metals [51].



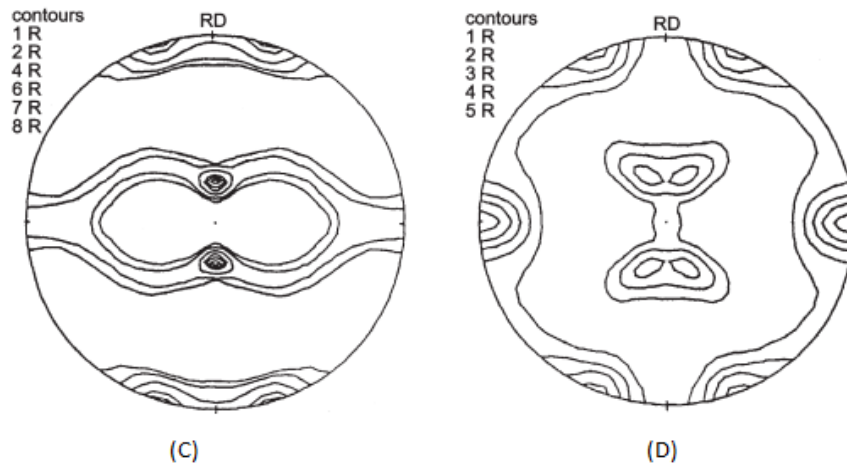


Figure-6: (c)  $\{111\}$  pole figures of 95% cold rolled copper and (d) 70:30 brass [41].

### 2.3 Recrystallization Texture of FCC metals:

When a cold deformed material is heat treated, the initial cold deformation texture will change during recrystallization and eventually during subsequent grain growth. This is called a ‘recrystallization texture’ or an ‘annealing texture’. These textures are responsible for the anisotropy in the mechanical properties of the material and determine the properties of the end products.

Recrystallization textures of fcc materials are influenced by several factors, like the amount of preceding cold deformation i.e. induced strain, the starting texture and microstructure, the purity of the metal, etc. Under favorable processing conditions (large rolling reduction, small initial grain size and sufficiently high annealing temperature), the main annealing texture component is the cube orientation  $\{100\} \langle 001 \rangle$  (Figure-7).

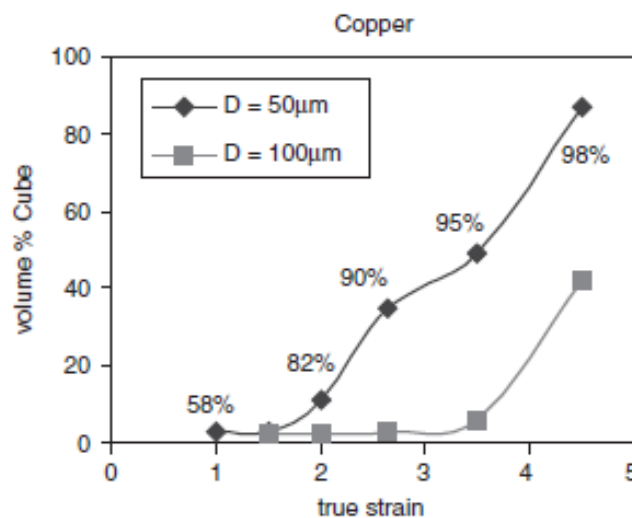
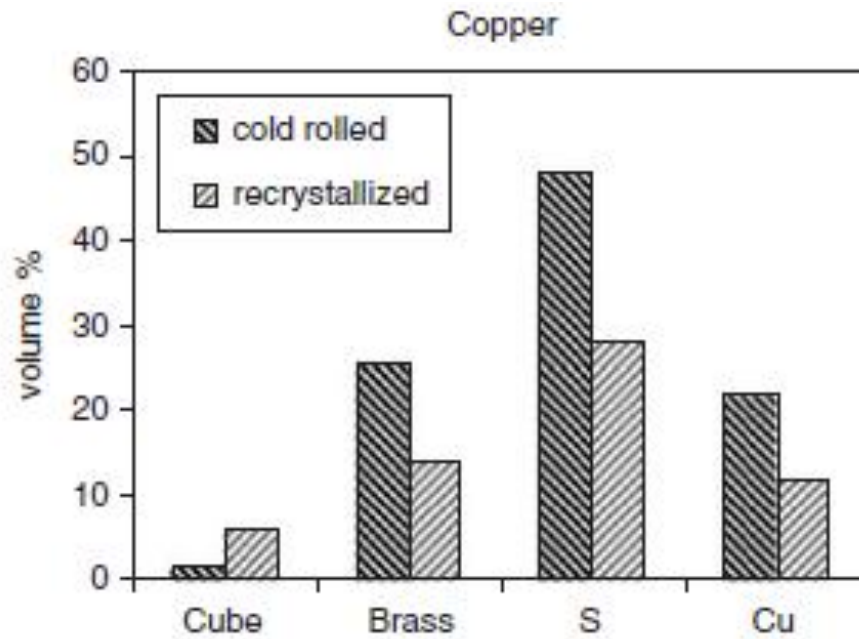


Figure-7: Volume percent cube in 99.995 wt% Cu in fully recrystallized condition, as function of hot-rolled grain size and cold rolling reduction [51].



**Figure-8: Some important texture components in 99.995 wt% Cu after 93% cold rolling and after recrystallization at 200° C [51].**

In pure Al also the same cube texture as in Cu can be found (Figure-8, Figure-9), thus here data are shown for copper and can be used as a reference for aluminium. Following table (Table-2) represents the recrystallization texture for fcc materials with their Euler angles and Miller indices.

**Table-2: Components of recrystallization texture in FCC metals [41].**

Notation	Miller indices	Euler angles		
		$\varphi_1$	$\Phi$	$\varphi_2$
Cube	$\{001\} \langle 100 \rangle$	0	0	0
-	$\{236\} \langle 385 \rangle$	79	31	33
Goss (G)	$\{011\} \langle 100 \rangle$	0	45	0
S	$\{123\} \langle 634 \rangle$	59	37	63
P	$\{011\} \langle 122 \rangle$	70	45	0
Q	$\{013\} \langle 231 \rangle$	58	18	0
R (aluminium)	$\{124\} \langle 211 \rangle$	57	29	63



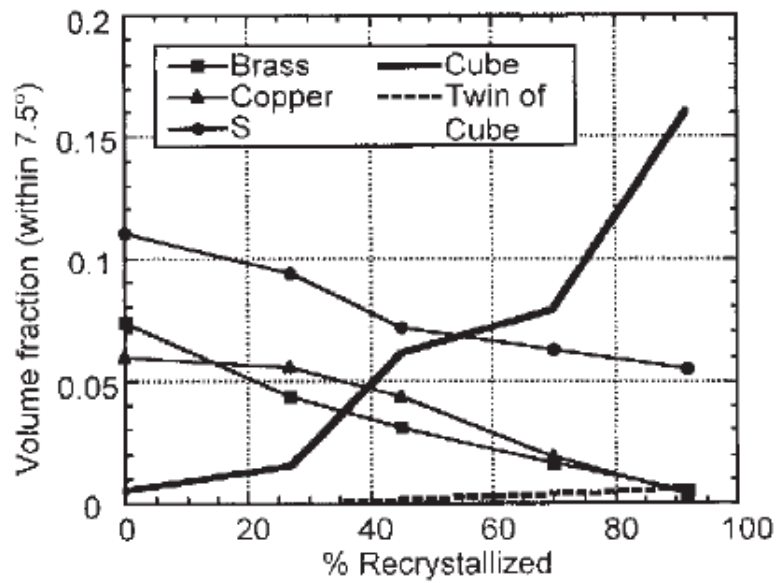


**Figure-9: plot of volume fractions of ideal components for copper with increasing recrystallization [51].**

The early work on commercial purity Al has shown, by analyzing  $\{111\}$  pole figures (Figure-10), that the texture developed after ARB is asymmetric and very weak [15]. Furthermore, for the same alloy, Hanson and Prangnell [38] revealed that most of the shear texture is rotated Cu and S textures when incorporated into the centre during ARB process. Another study by Kim et al. [57] observed the presence of ideal Cu and Dillamore  $\{4,4,11\}\langle 11,11,8 \rangle$  orientations at the centre of the strip after ARB, demonstrating that the texture of ARB-processed sheet has more complex features than that of conventionally rolled sheets.

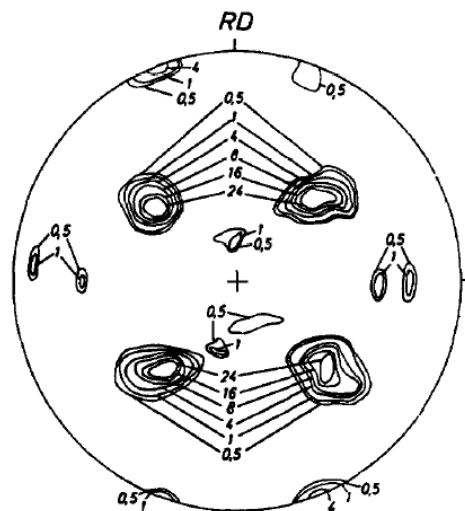


**Figure-10:  $\{111\}$  Pole figure of heavily deformed and recrystallized 99.99% Aluminium [51].**

Materials with a high SFE like Al, Ni, and Cu typically form a cube recrystallization texture  $\{001\}\langle 100 \rangle$ ; an example is shown in Figure-11. The mechanisms leading to the cube recrystallization texture have been subjected to debate for more than six decades; a systematic review of this research is given by Hu (1986). Only with the advent of techniques for micro texture analysis, the nucleation and growth mechanisms of cube-oriented grains have been understood quite comprehensively.

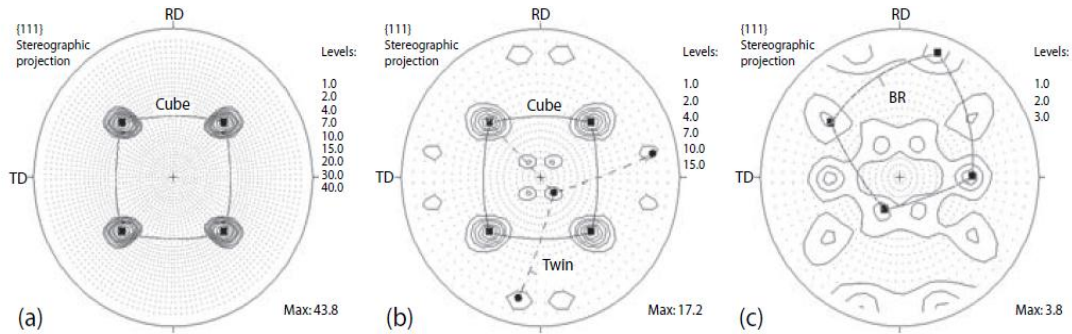


**Figure-11: Recrystallization texture of cold rolled FCC metals (a) aluminium, (b) copper, and (c) brass (Cu-37%Zn) ( $\{111\}$  pole figure) [58].**

## 2.4 Why Al and its alloys?

The main objective of the transportation and automotive industry is fuel reduction, and hence energy saving. In vehicles, there are many components such as engine, body, air conditioner; seats etc. which contribute to the additional weight in vehicle. The aim is, therefore, to reduce the overall vehicle weight by using lightweight materials or thinner materials without compromising in strength and safety. Additionally, developed lightweight material should be of lower cost.

In recent years, aluminium and its alloys have attracted attention of many researchers and engineers as it is promising materials for automobile industry and aerospace application [43-45]. Such as, 6xxx graded aluminium have advantages, medium strength, formability, weld ability, corrosion resistance and low cost. In the modern era steels is substituted by aluminium which result in great improvement in energy economy, recyclability and life-cycle cost [44-46]. It is reported that the ARB processed materials shows outstanding tensile strength. Therefore, ARB processed aluminium alloys is the promising material for automobiles, because it is of light weight and with high tensile strength.

Audi is the first company, who is using this concept and producing completely aluminium auto body using aluminium space frames and tailored blanks [figure-12] on mass scale.

Tailored blanks are made up of two or more metal sheets of unequal thickness, which are welded together to form a single blank and which can be subsequently used for sheet metal operations such as bending, stretching, deep drawing, etc. Tailored blanks have a load optimized design and therefore, are less damageable in the case of accident [47]. From Later on BMW group also recognize the advantages of aluminium with the development of its 5<sup>th</sup> series vehicles.



**Figure-12: Audi A8 with an aluminium space frame and tailored blank door structure for weight reduction [48].**

# Chapter 3

## Objectives of the present work

Nanostructured or ultrafine grained aluminium plays an important role in making of the high strength-lighter body automobile parts, enabling them to withstand collision without fatal hurting the inside passengers. However, annealing of UFG aluminium may cause coarsening of grains with certain crystallographic texture, leading to softening of the metal and is deterministic for its structural applications. Therefore, it is imperative to study and analyse annealing effects on ultra-fine grain aluminium materials and tailor-out of its related thermal processing factors for best usages.

- (a) To understand the basic scientific details of ARB producing UFG and annealing effects in aluminium related materials utilized in the industry, ultra-pure aluminium (99.999 wt%) “C” and commercially pure aluminium (99.5 wt%) “A” sheets are used.
- (b) Microstructure-texture evolution studies from one ARB cycle (AC-1) to ten ARB cycles (ARB-10) were performed.
- (c) For annealing heat treatments from 150 °C to 450 °C followed by quenching of AC-1 to AC-10 specimens are done.
- (d) Further microstructure-texture evolution studies of annealed specimens from one ARB cycle (AC-1) to ten ARB cycles (ARB-10) were performed.

The above mentioned objectives are analyzed through hardness values, grain boundaries types, microstructure and crystallographic texture components of accumulative roll bonded aluminium composite laminates of different purities before heat treatment and after annealing at various temperature.

# Chapter 4

## Experimental process

### 4.1 As-received Sample and its Cutting

This chapter introduces the materials and experimental techniques used in this study. In this study, highly pure aluminium (99.999 wt. %) and commercially pure aluminum (99.5 wt. %) after annealed at 500° C for 1 hour and roll bonded up to 10 rolling cycles, is chosen and investigated, which were used as a starting material. All these sheets were 1 mm thick.

ARB sheets of above mentioned commercially pure aluminium (called as “A”) and highly pure aluminium (called as “C”) used as starting materials for the study. These sheets named as AC1 to AC10 according to their rolling cycle. Here “A” represent alloy aluminum and “C” represents highly pure aluminum and digits from 1-10 represents number of ARB cycles. These sheets of particular rolling cycles are cut into various small pieces of size  $\approx 1 \times .7$  cm using Struers Secotom-15 precision cutting machine and “SBT MODEL-650 low speed diamond wheel saw”.

### 4.2 Annealing:

These small pieces of various ARB cycled aluminium sheets are heat treated in salt bath furnace (“THERMOTHERM”) from 150° C to 450° C with 25° C temperature intervals, to study static recrystallization behavior. Initially, in salt bath furnace the desired temperature was maintained and the samples are hanged inside the molten salt, where the temperature is measured by installed thermocouples.

After keeping the samples for 30 minutes, samples are taken out from salt bath and water quenched immediately. Same process was repeated for each ARB rolled cycles samples (AC-1 to AC-10) with increasing temperature 25° C.

### 4.3 Hot Mounting:

After cutting the samples, the next step is mounting. The objective of this step is to handle small or odd samples and to protect fragile materials, thin layers or coating. It produces samples with uniform size and shape so that it is better for holding and further preparation processes. Samples were hot mounted using Multifast-Black Bakelite powder and “Struers CitoPress-10” instrument.

For each sample mount using 45 ml Multifast Black Bakelite powder temperature, pressure, heating time and cooling time were kept at 180° C, 250 bar, 4 minutes and 4 minutes respectively.

#### **4.4 Grinding and Polishing:**

Grinding and polishing is the very crucial step for sample preparation. Through grinding damaged or deformed surfaces or saw marks of the sample can be removed. On the other hand polishing removes the surface artifacts of grinding. In this study we have used manual polishing machine “ATA SAPHIR-330” and “Struers LaboPol-5”, and automatic polishing machine “Struers Tegramin-25”. For grinding SiC abrasive papers of grit size 500 to 2000 were used and for polishing 6µm, 3 µm and 1 µm diamond suspension were used.

#### **4.5 Micro-hardness Test:**

Micro-Hardness tests are used to determine the hardness of a material. Hardness of the materials generally correlates linearly with ultimate tensile strength. Therefore, it can be used as a measurement of the mechanical property of materials. In this study “emco TEST Dura Scan” Vickers hardness instrument were used. Vickers hardness test consist of a square-base diamond pyramid indenter with the opposite faces of pyramid 136°.

By measuring the two diameters of faces of indent on metals, we can calculate Vickers hardness (kgf/mm<sup>2</sup>) according to following equation:

$$HV = 2F \sin \frac{136^\circ}{2} \left/ \left( \frac{d_1 + d_2}{2} \right)^2 \right.$$

In this project study the load was fixed at HV 0.025 and dwell time at 15 second.

#### **4.6 Electro polishing:**

In this project metallographically ground specimens are electro polished at 42 volt voltage using etchant mixture of 91 wt. % pure ethanol and 9 wt. % per chloric acid. This etchant was cooled up to -20 °C to -17 °C using liquid nitrogen and sample was dipped in this etchant for 12 to 15 seconds for three times and simultaneously observed the smooth and shiny surface. After good polishing these samples were stored in separate small vials of acetone solution.

For removal of undesired small particles these samples are ultrasonically cleaned for 15 minutes and dried with air blower. Now, these samples are mounted on separate stubs by using silver paste as glue.

#### **4.7 Electron Backscattered Diffraction (EBSD) attached in Scanning Electron Microscopy (SEM):**

EBSD is a microstructural-crystallographic characterization technique used to examine the crystallographic orientation of crystalline materials, used to determine their texture or preferred orientation. We performed this on SUPRA 40 with ZEISS SEM machine. A source of electron beam when focused on thick crystalline material, electron backscattered diffraction pattern also called Kikuchi pattern is generated which is then acquired by the camera and matched with the computer generated Kikuchi pattern of the input crystal system specification by the software and the crystal orientation is determined. When this step is repeated after regular interval of distance while scanning over the sample surface, an orientation image map containing variety of crystallographic details is obtained by using HKL Channel 5<sup>®</sup> software. Further analyses of high angle grain boundaries, crystallographic texture, etc were also performed using the same software.

# Chapter 5

## Results and discussion

### 5.1 Initial Specimens

The as-received initial aluminium sheets of commercial purity (A0) and high purity (C0) which are rolled and homogenized at 500 °C for 1 hour, were metallographically polished on their planes perpendicular to the transverse direction (i.e. containing normal direction and rolling direction) and SEM (BSE and EBSD) studies were performed on these surfaces (center region of the surface). These initial as-received sheets are noted as A0 BHT and C0 BHT where BHT is the acronym of before heat treatment. Number fraction of HAGBs, EBSD maps and fraction of microtexture components (only two grains noticed in C0) are calculated by the HKL Channel-5® software. Figure-13 shows the EBSD maps obtained from these as-received sheets.

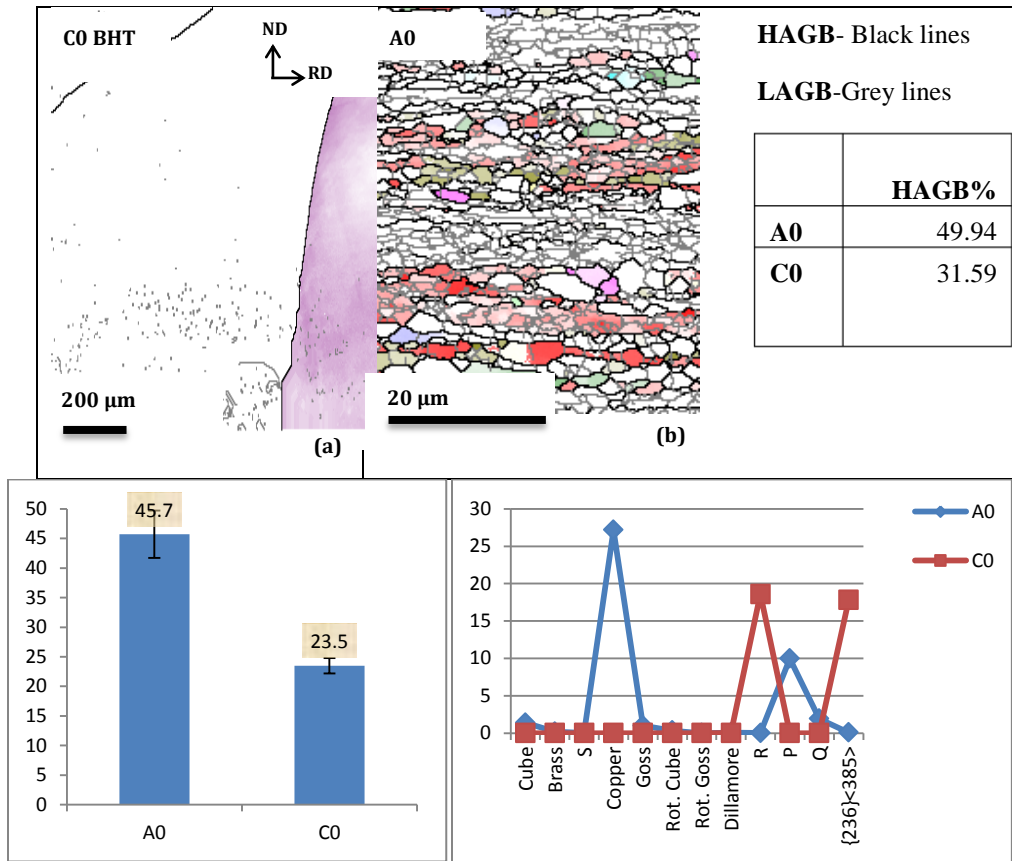


Figure-13: (a) EBSD orientation maps of highly pure aluminium, C0 (b) commercially pure aluminum, A0 with (C) hardness plot for A0 and C0 and (d) volume fraction of various texture components.



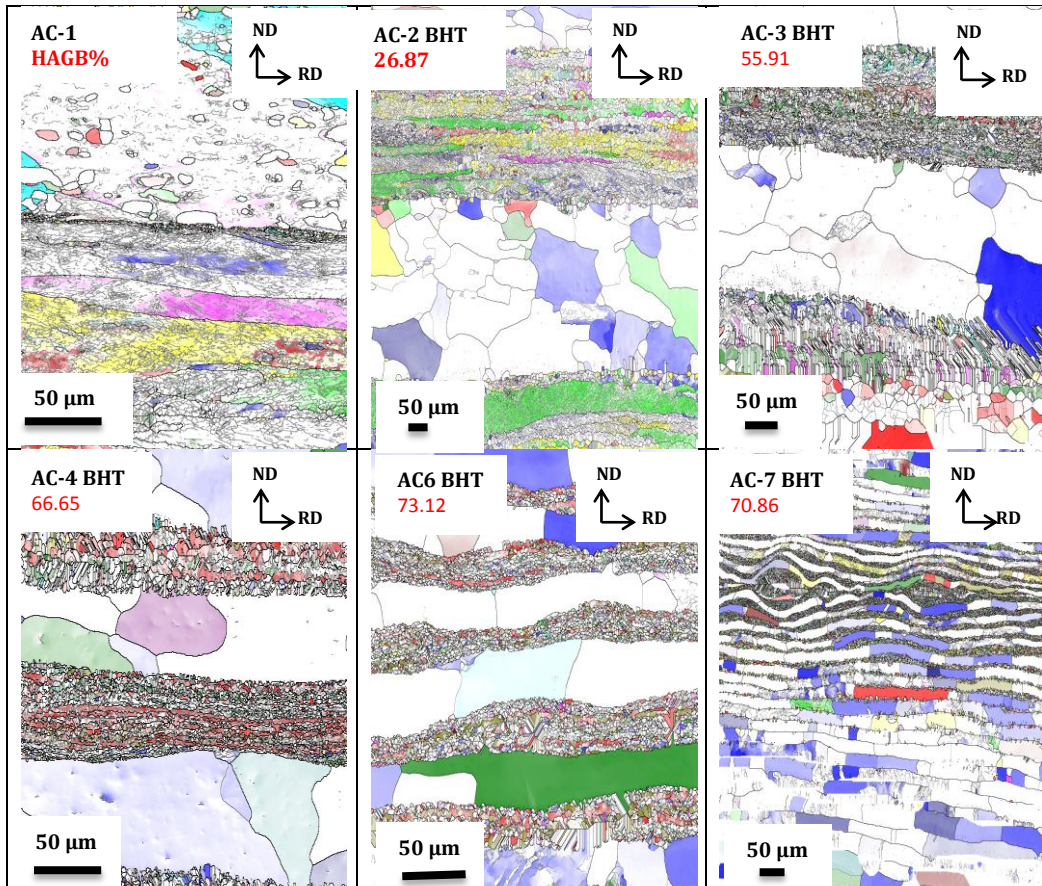
The high-angle grain boundaries with misorientation angles above  $15^{\circ}$  are shown as black lines, while boundaries between  $2^{\circ}$  and  $15^{\circ}$  are shown as grey lines. Boundaries below  $2^{\circ}$  are not included due to the uncertainty in the determination of low-angle misorientations using EBSD. The number fraction of high angle grain boundaries (HAGB) and low angle grain boundaries (LAGB) are about 50% and 32 % respectively in commercially pure aluminium (A0) and highly pure aluminium (C0).

Very coarse grains of 1mm range are found in the C0 sheet whereas several  $10\ \mu\text{m}$  range grains are noticed in A0 sheet. For the microtexture classification, the tolerance angle from each ideal orientation was set at  $15^{\circ}$ . The microtexture noticed, from these small area shown maps, are  $\{112\}\langle 111\rangle$  (copper) and  $(011)[122]$  (P) for commercially pure aluminium sample (A0) and  $(124)[211]$  (R) and  $\{236\}\langle 385\rangle$  for highly pure aluminium (C0) sample.

The hardness of commercially pure aluminium (A0) is measured 45.7 VHN and nearly half of it is noticed in commercially pure C0 aluminium (23.5 VHN).

## 5.2 ARB specimens (AC-1 to AC-10)

Similar studies are performed of ARB specimens (AC1 to AC10) and their EBSD maps, number fraction of high angle grain boundary details, hardness values and microtexture results (standard fcc rolling and recrystallization texture components) are given in Figure.



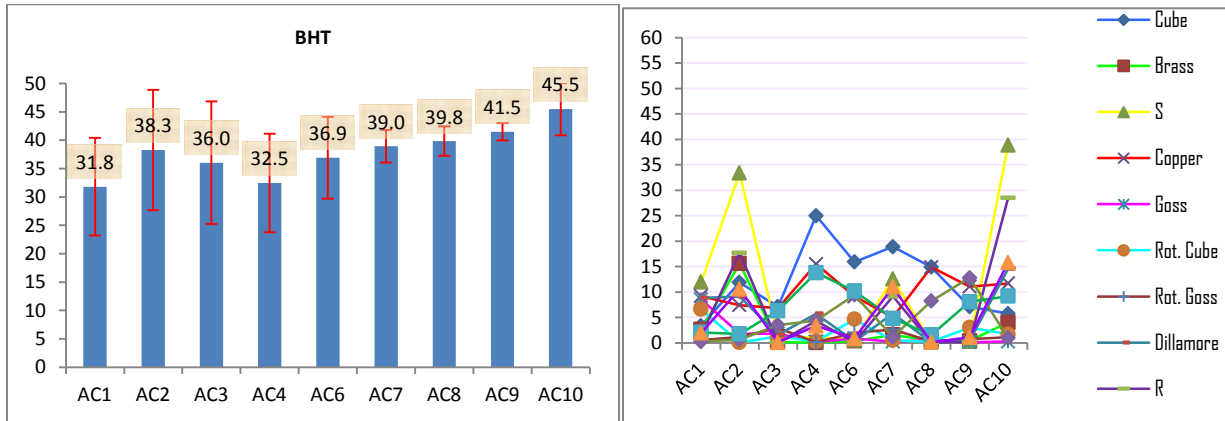
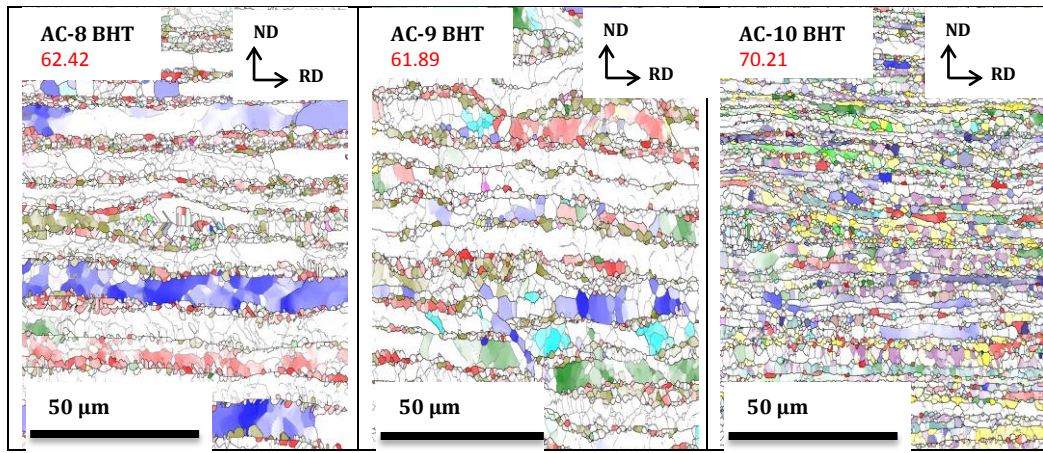


**Figure-14: EBSD maps of AC-1 to AC-10 ARB cycled aluminium samples with their corresponding hardness value plot and microtexture component graphs.**

From the above given figure, it is found that in AC-1 specimen (one A0 and one C0 sheets are roll bonded up to 1 mm thick) the highly pure (C-sheet) are deformed with nucleation of few smaller grains. This is due to very high purity of aluminium which has initiated dynamic discontinuous recrystallization [59].

While in the commercially pure layer (A-sheet), typical rolled lamellar structure is formed. However, in this layer intense low angle grain boundaries and dislocations tangles are observed which are surrounded by the lamellar structure of original grains.

With the increase in ARB cycles (in the 2 cycle ARB samples) it is observed that in the A layer during deformation the dislocations are generating and due to dynamic recovery some subgrains are formed. In this layer the lamellar structures becomes thinner and some grains are evolving due to continuous recrystallization. Whereas, in C layer the grains are now nearly fully recrystallized. The nucleated grains in C layer of AC-1 are now coarsened. On the basis of HAGB number fraction value it may be suggested that in C layer HAGB increases but there are still few LAGB present within the grains. Whereas, in the A layer dislocations (LAGB) arranged themselves into sub grains. Hardness plot also suggests that due to more deformation and grains refinement average hardness of the sheet is increased.

Similar trend is observed in AC-3 specimen as well with more continuously recrystallized grains generated from the lamellar grains in the A layer, resulting into little decrease in hardness. A sharp rise in HAGB and decrease in hardness also indicate increase in recrystallization.

In AC-4 specimen, continuous recrystallized grains are in the A layer whereas in the C layer the grains sizes are free of internal misorientation and are adjusted according to its rolled laminate layer size, becoming cellular-longitudinal grains elongated along the rolling direction. Volume fraction of HAGB is nearly double compared to AC-2.

Thus it can be predicted that here in this cycle continuously recrystallized grains in A layer increases and with internal misorientation-free C layer grains, AC-4 provided decreased hardness value.

In AC-6 nearly all the A layer grains are small equiaxed achieved through continuous recrystallization whereas in C layer compartmentalization of the grains occurred up to its boundary layer i.e. grains with rectangular shape evolved. It is interesting that still there is no mixing of grains and still both the layers can be identified separately. Average hardness started increasing due to the development of more fine grains than the previous ARB cycled specimens. The volume fraction of HAGB also increased suggesting about increased dynamic recrystallization.

More refined heterogeneous microstructure with smaller grains is noticed in AC-7 specimen. The C layer contained complete compartmentalized elongated grains and A layer grains whenever seen are very refined. It may also be observed that some A layers are consumed by pure C layer by large deformation and from this cycle onwards the grain mixing can be seen. This resulted into slight decrease of HAGB with slight increase in hardness.

Eight cycles ARB (AC-8) and nine cycles ARB (AC-9) EBSD maps are very similar looking in microstructure and number fraction of HAGB. In both of these specimens, the pure C layer grains started fragmenting and becoming similar in size and mixed with the coarsened A layer grains. The small angle fragmentation of grains in the C layer decreased the HAGB fraction but in turn increased the hardness to slightly higher value.

Ten cycles ARB (AC-10) EBSD map analysis suggests the development of very fine fully recrystallized grains microstructure. The previous cycle generated small angle misoriented grains in C layer are now separated by HAGB. For this cycle prediction of separation of alloy and pure layer is difficult. These ultra-fine grains are elongated in the rolling direction and number fraction of HAGB and hardness of this sheet increases significantly when compared to the lower cycles ARB samples.

Generally, the HAGB number fraction is directly related with the recrystallized amount in the microstructure. For as received samples of ARB-1 to ARB-10, number fraction of HAGB with respect to ARB cycles is plotted and is shown below. The points fit line with polynomial function of the order three is also given.

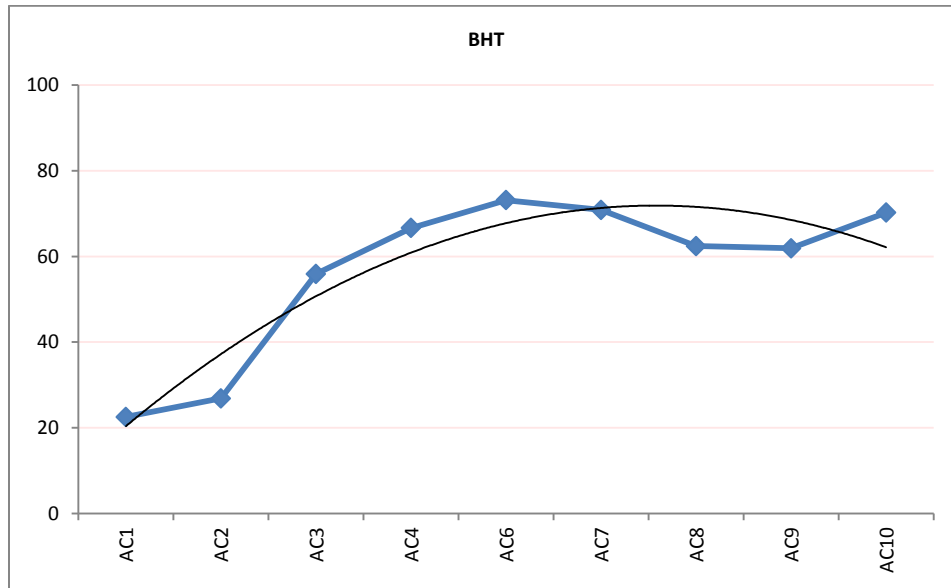


**Figure-15: For as received samples Number fraction of HAGBs with ARB cycles.**

The trend in the above plot clearly shows the increase of HAGB fraction with increased ARB cycles up to nearly AC-6 and then decrease of HAGB fraction with more ARB cycles (up to AC-9) and then increase again in AC-10. This trend can be explained by the fact that all through ARB cycles up to AC-6, the A layer was under continuous recrystallization and the pure C layer was under discontinuous recrystallization, mainly generating grains with HAGB. From 7 cycles onwards, fragmentation of pure C layer grains into LAGB decreased the recrystallized amount. With fully developed ultra-fine grains with HAGB in AC-10, the increase in recrystallized fraction can be thought. The initial trend of the present results (increase-decrease) of recrystallized amount matches quite well with Chekhonin et al [59] where they directly calculated the recrystallized grain amount through BSE images. Only their findings of last decrease in recrystallized fraction are not matching with the present results.

### 5.3 Texture Evolution from AC-1 to AC-10

From all through the ARB cycles the pure C layer always contained mainly cube texture (blue color in Figure-14) with additional few Goss, Rot. Cube and Q components. It is very general to obtain Cube component during discontinuous recrystallization and grain growth upon annealing of FCC materials. Interestingly, additional shear Cube component is also observed shifted as a whole by  $15^\circ$  by the applied shear on the surface. Chekhonin et al [59] also noticed similar shear by higher values and reasoned it because of the simple shear due to friction between the rolls and the specimen surface in the previous ARB cycle.

Whereas A layer (commercial pure Aluminium) Copper type and S type components which are typical FCC deformation texture components in the earlier ARB cycles (can be seen in elongated deformed lamellar grains in Figure-14). Later on, these Copper and S type components persists in the later ARB cycles through generated smaller grains by dynamic continuous recrystallization. In dynamic continuous recrystallization, there is some rotation of sub-grains with not much change in (see Appendix 1 for more details). Also observed are shear Copper and Shear S components (sheared  $15^{\circ}$ - $20^{\circ}$ ) in good amount which are also similarly reported by Hanson and Prangnell et al.in ARB commercial pure aluminium [38].

#### **5.4 Annealing Effects:**

The annealing effects of AC-1 to AC-10 specimens heat treated from  $150^{\circ}\text{C}$  to  $450^{\circ}\text{C}$ , studied through SEM-EBSD orientation maps, hardness values and microtexture details of the area perpendicular to the transverse direction of the sample are presented and discussed below. The EBSD orientation maps show the colored texture components (standard FCC rolled and recrystallized) with a tolerance up to  $15^{\circ}$ , also with LAGB ( $2^{\circ}$  to  $15^{\circ}$ ) and HAGB ( $> 15^{\circ}$ ) represented with grey and black lines. HAGB number fraction is also mentioned in the map. This is followed by hardness values measured and microtexture found in each annealed specimen.

**Microstructure, hardness and texture evolution of annealed accumulative roll bonded samples (from AC-1 to AC-10).**



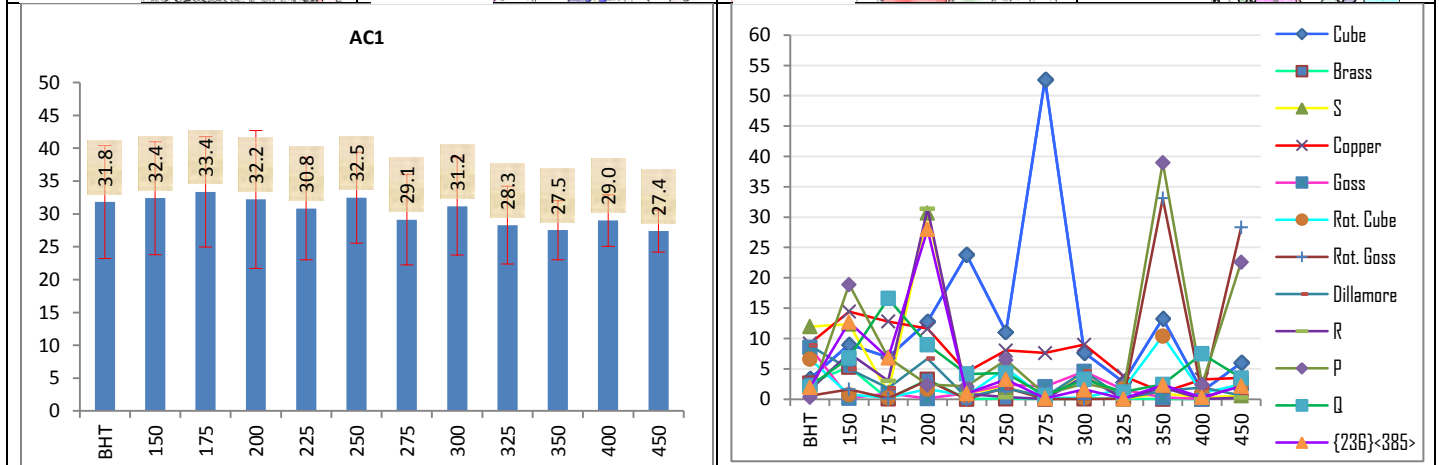
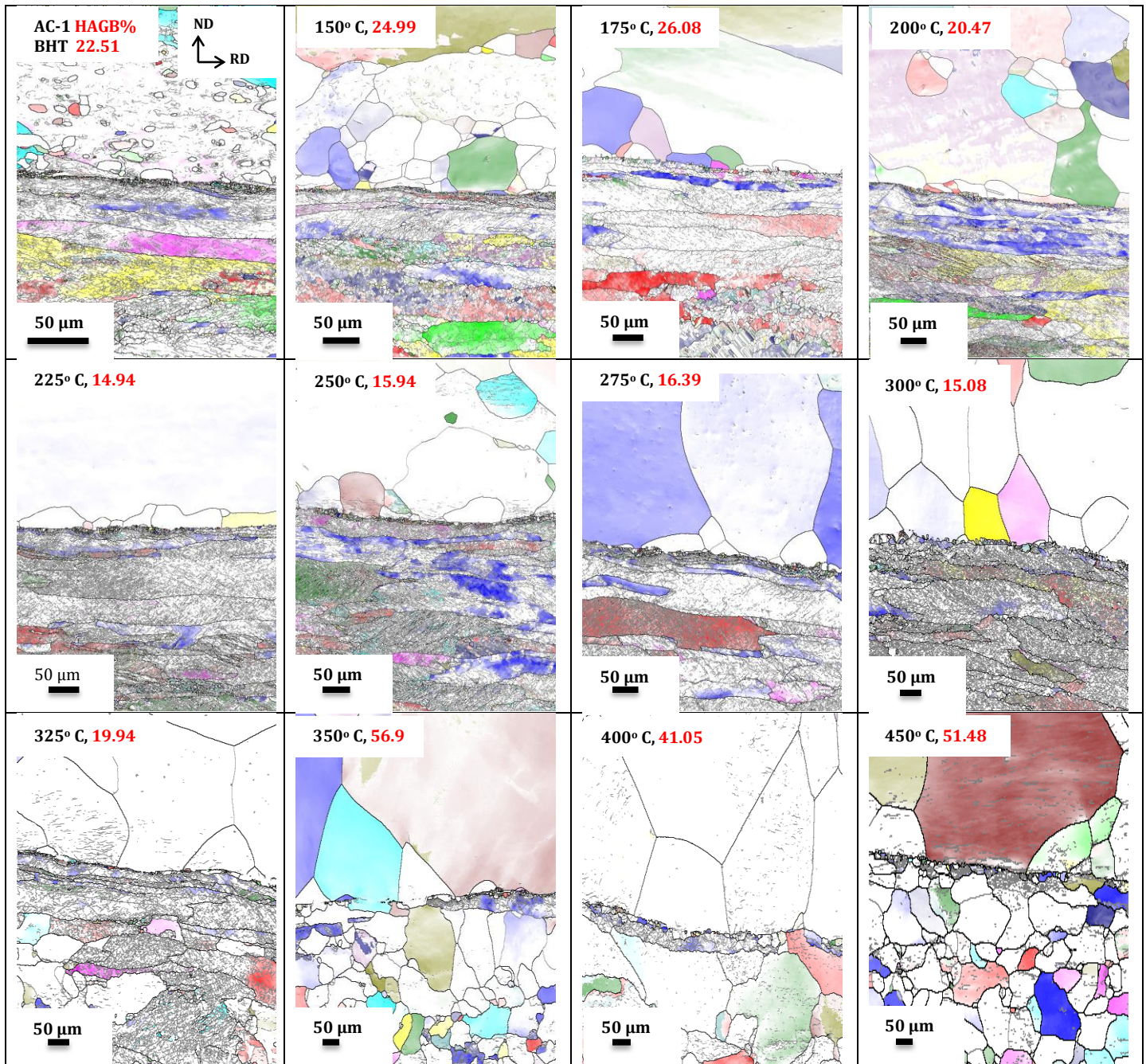


Figure-16: EBSD orientation maps, annealing temperature vs. hardness plot and annealing temperature vs. volume fraction of texture components for AC-1.



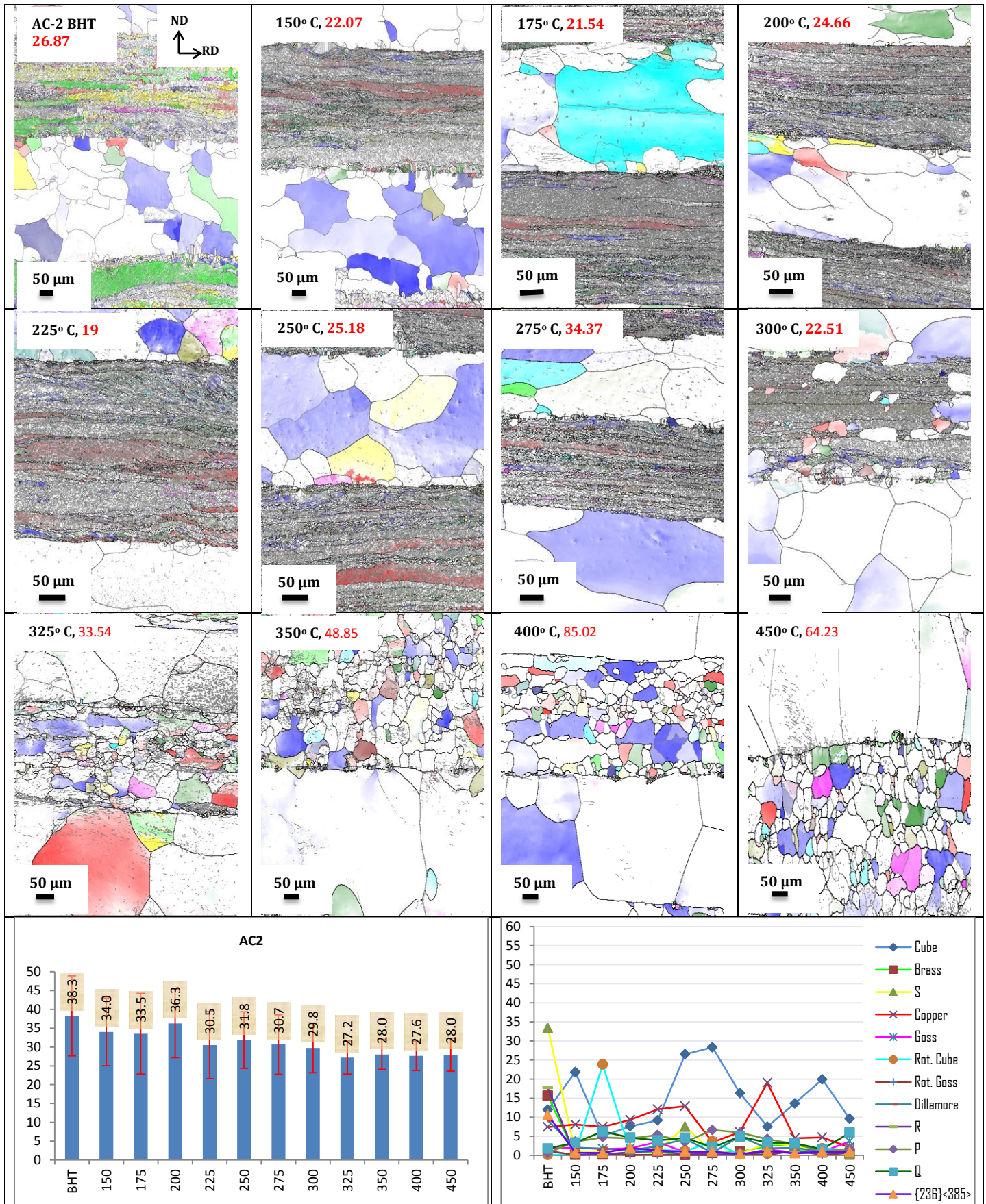


Figure-17: EBSD orientation maps, annealing temperature vs. hardness plot and annealing temperature vs. volume fraction of texture components for AC-2.











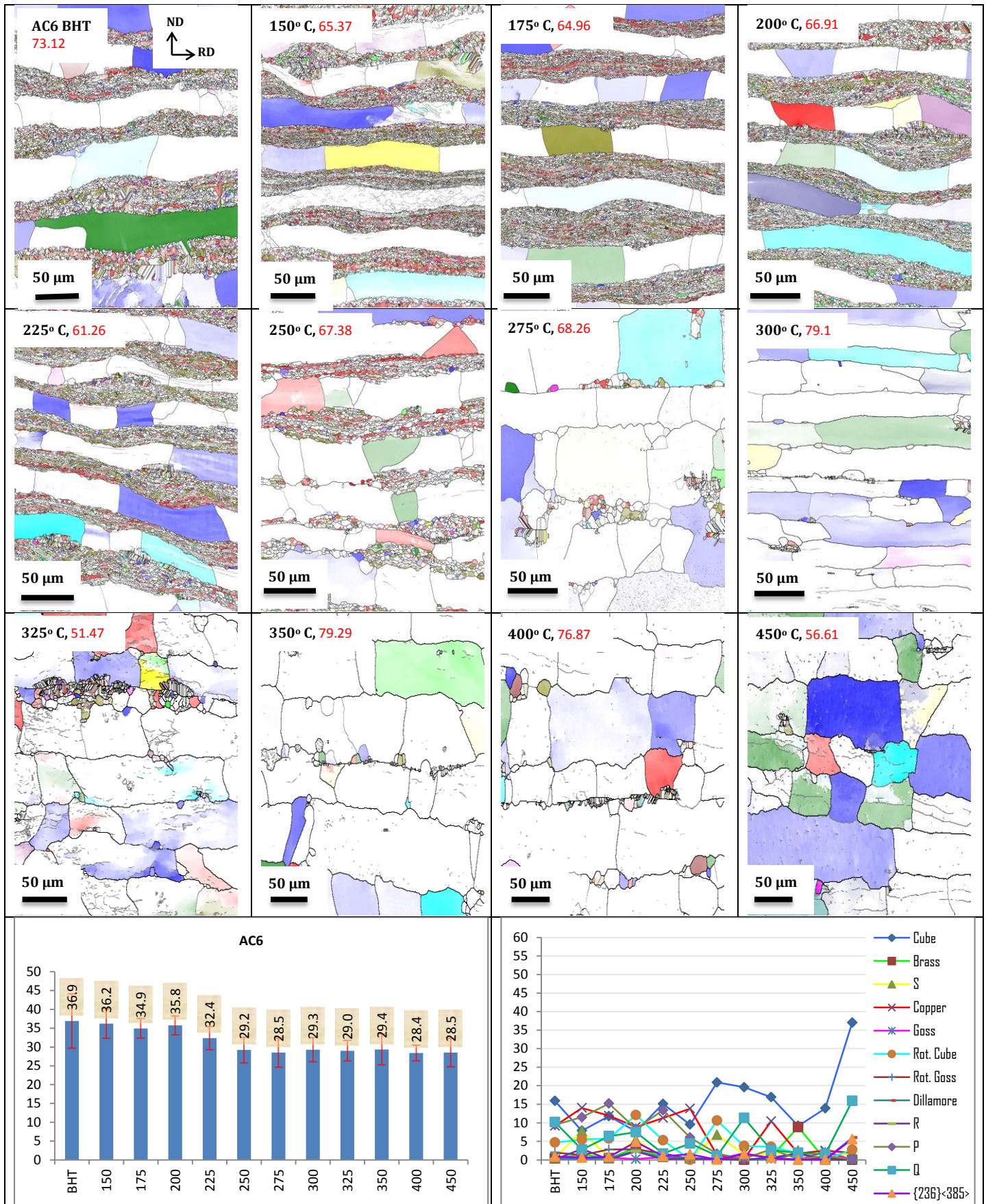


Figure-20: EBSD orientation maps, annealing temperature vs. hardness plot and annealing temperature vs. volume fraction of texture components for AC-6



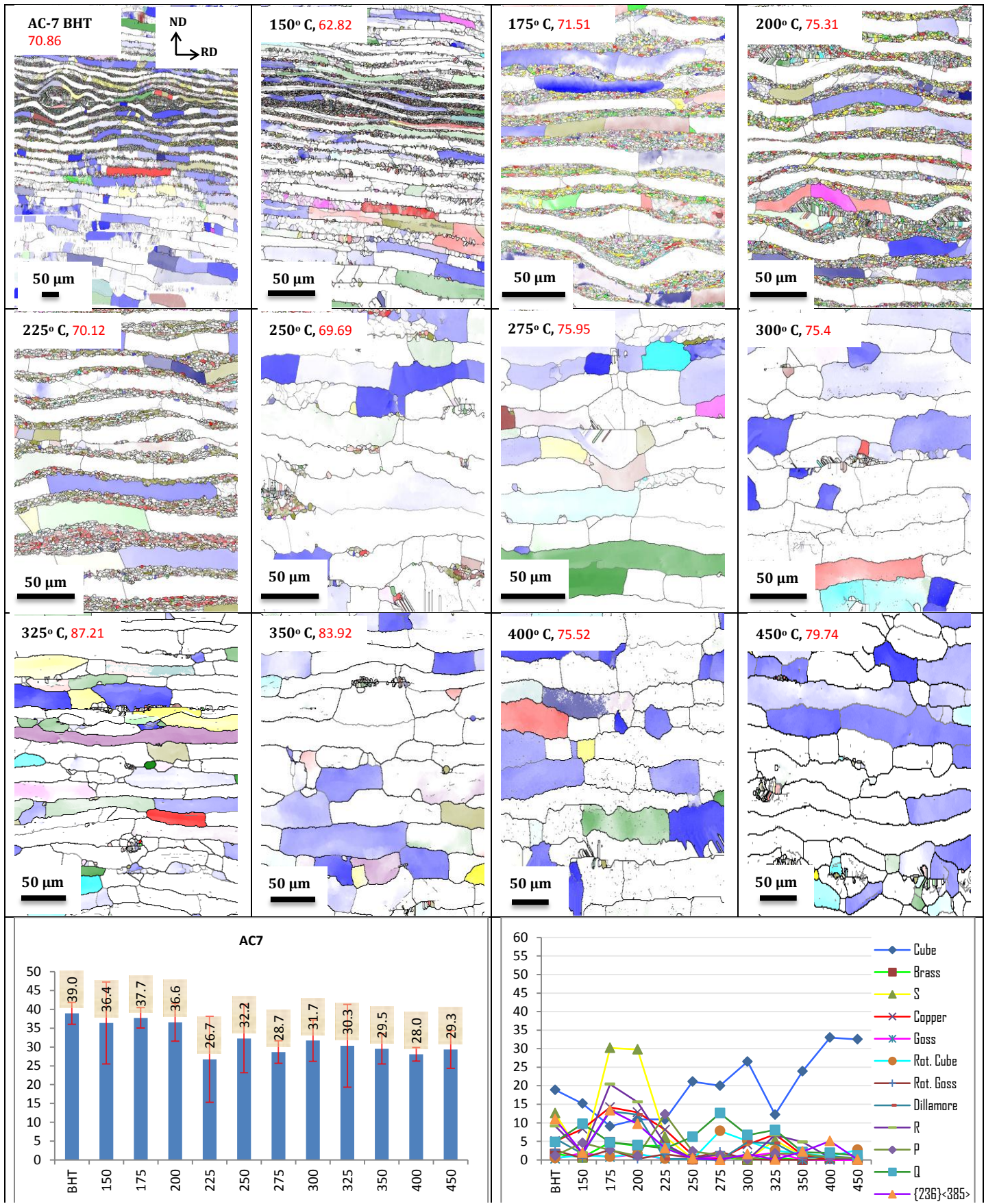


Figure-21: EBSD orientation maps, annealing temperature vs. hardness plot and annealing temperature vs. volume fraction of texture components for AC-7







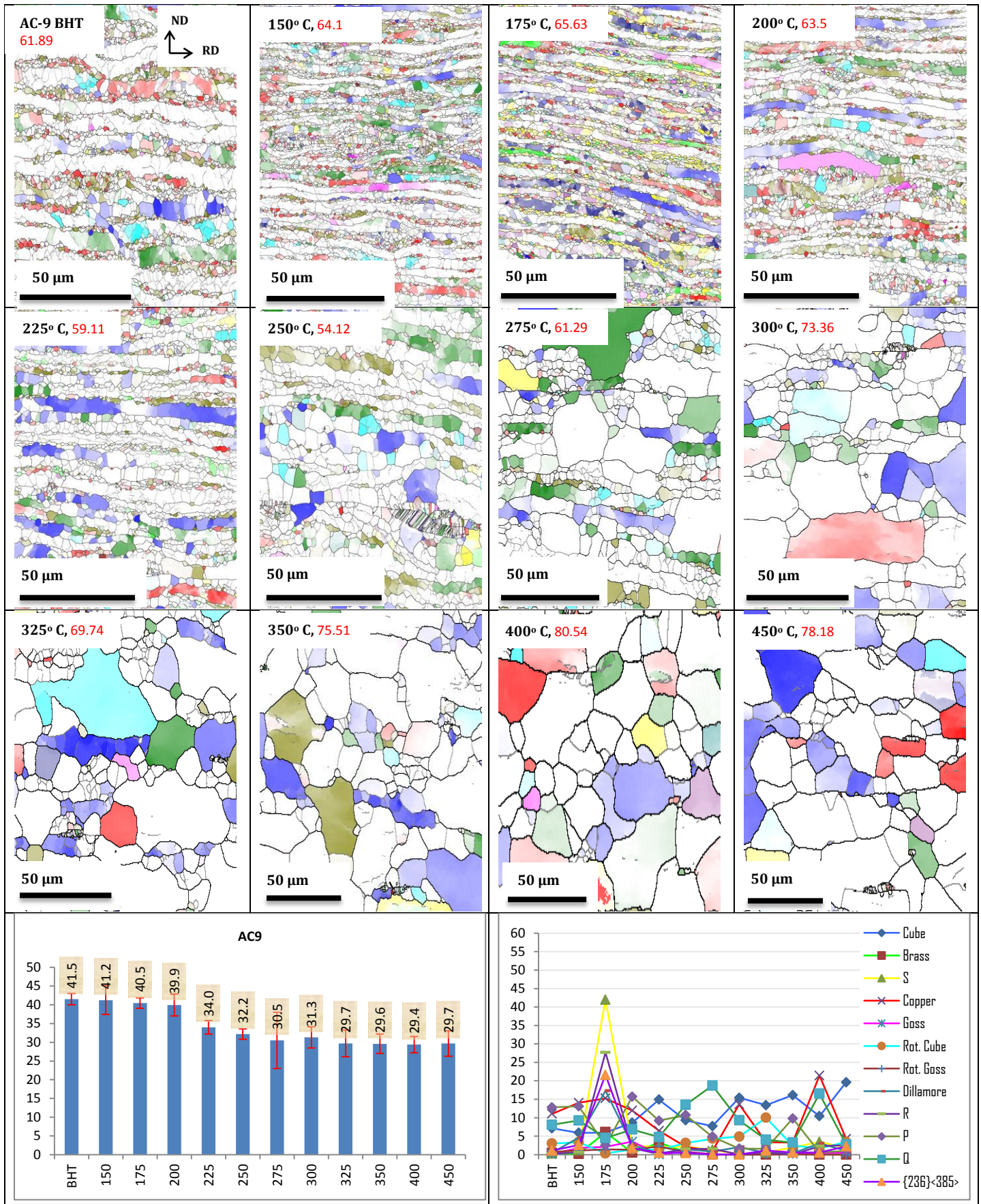


Figure-23: EBSD orientation maps, annealing temperature vs. hardness plot and annealing temperature vs volume fraction of texture components for AC-9



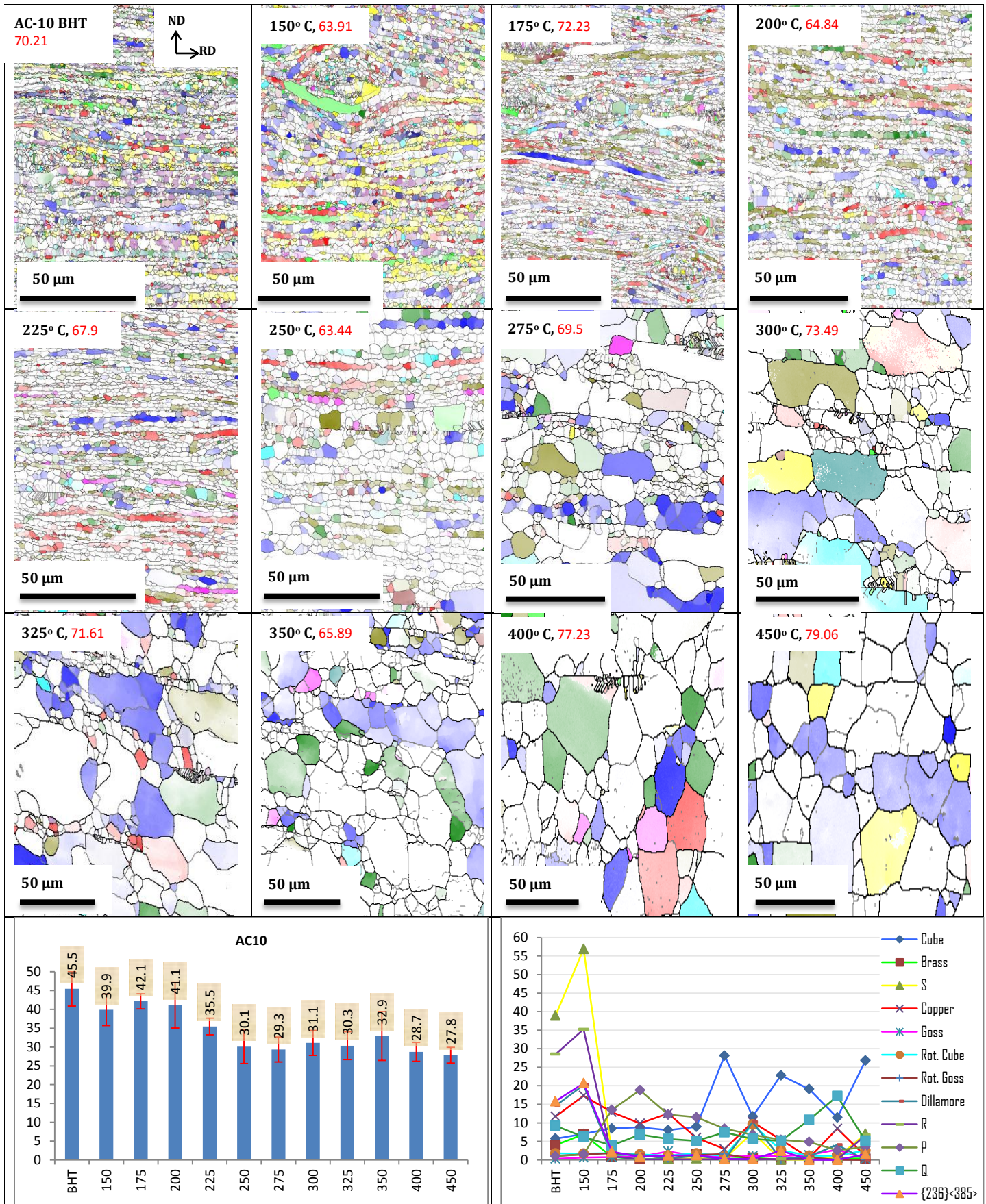


Figure-24: EBSD orientation maps, annealing temperature vs. hardness plot and annealing temperature vs volume fraction of texture components for AC-10

The before heat treatment microstructure details of one cycle ARB sample (AC-1) is discussed in the previous section where the high purity C layer is observed containing large grains having dislocations with smaller grains nucleated inside the large grains and the commercially pure A layer is seen having deformed rolled lamellar structure with high dislocations and LAGBs inside. When this specimen is annealed from 150 °C to 450 °C temperature for 30 minutes with an increment of 25 °C at each annealing step, grains in the C layer become more recovered, recrystallized with coarsening of the earlier AC-1 (before heat treatment) generated small nucleated grains and generation of recrystallized grains from 325 °C onwards with its coarsening in the deformed lamellar grains of A layer. This has also been noticed by the increase in HAGB values with annealing as well. Finally at 450 °C annealing, a bimodal layered equiaxed grain microstructure is generated, where the pure C layer is filled with large equiaxed grains and is separated by A layer with smaller equiaxed grains.

Similar to the annealing of AC-1 specimen, AC-2 annealing also underwent complete recrystallization of pure C layer with large grains and A layer with comparatively smaller coarse grains.

Recrystallization in A layer started at 300 °C onwards. This can be seen by the continuous increase in HAGB fraction and decrease and then constant hardness values with annealing temperature as well.

Like the annealing of AC-1 and AC-2, AC-3 annealing developed into similar bimodal layered equiaxed grains microstructure still maintaining distinct different A and C layers through their grain sizes. The recrystallization of A layer grains started from 275 °C onwards.

In AC-4 annealing, recrystallization of grains and its coarsening started from 250 °C onwards. Additional effects are seen from 300 °C onwards where the large grains of pure C layer are noticed to enter towards the normal direction into the A layer region and started consuming the small recrystallized A layer grains. Still by the 450 °C the bimodal layered equiaxed grain microstructure is maintained with thinner A layer grains. HAGB fraction is also seen increased with annealing temperature.

In AC-6 before heat treated specimen, coarse rectangular compartmentalized grains are noticed in the pure C layer with small dynamically continuous recrystallized grains in A layer. Annealing shown the consumption of small A layer grains by the pure C layer grains which stretched the rectangular compartmentalized grains of C layer into square shape. This consumption of A layer grains is seen from 250 °C annealing.

Similar annealing effects is seen in AC-7 specimen with complete annihilation of A layer grains by pure C layer grains (can be seen from 250 °C onwards), generating compartmentalized elongated lamellar grains.

ARB AC-8 specimen showed fragmentation of large C layer grains with several LAGB. With low temperature (150 °C) annealing recovery of fragmented C layer grains took place. Further high temperature annealing started consumption of A layer grains by these C layer grains with some coarsening.

ARB AC-9 microstructure shown of fragmented grains in pure C layer with starting of consumption into the A layer grains. Low temperature (150 °C to 225 °C) annealing of AC-9 completed the annihilation of A layer grains by C layer grains. Further high temperature (275 °C onwards) annealing started coarsening of these grains into coarse equiaxed microstructure. There is a complete change from layered microstructure having distinguishable A layer and C layer grains (ARB AC-9 BHT) to coarse grained equiaxed microstructure at 450 °C. The change in hardness from high to stable low values also described the same.

Similar annealed microstructure of AC-9 is seen in AC-10 as well.

Overall, through annealing there has been significant change in microstructure seen: from earlier distinguishable A layer and C layer recrystallized grains of different sizes, followed by consumption of A layer small grains by C layer large grains and the final coarse equiaxed grain microstructure. This change in microstructure is ably reflected by their HAGB vs temperature plot (Figure-25). With increase in ARB cycles the spacing between the HAGB values are decreased for all annealing temperatures.

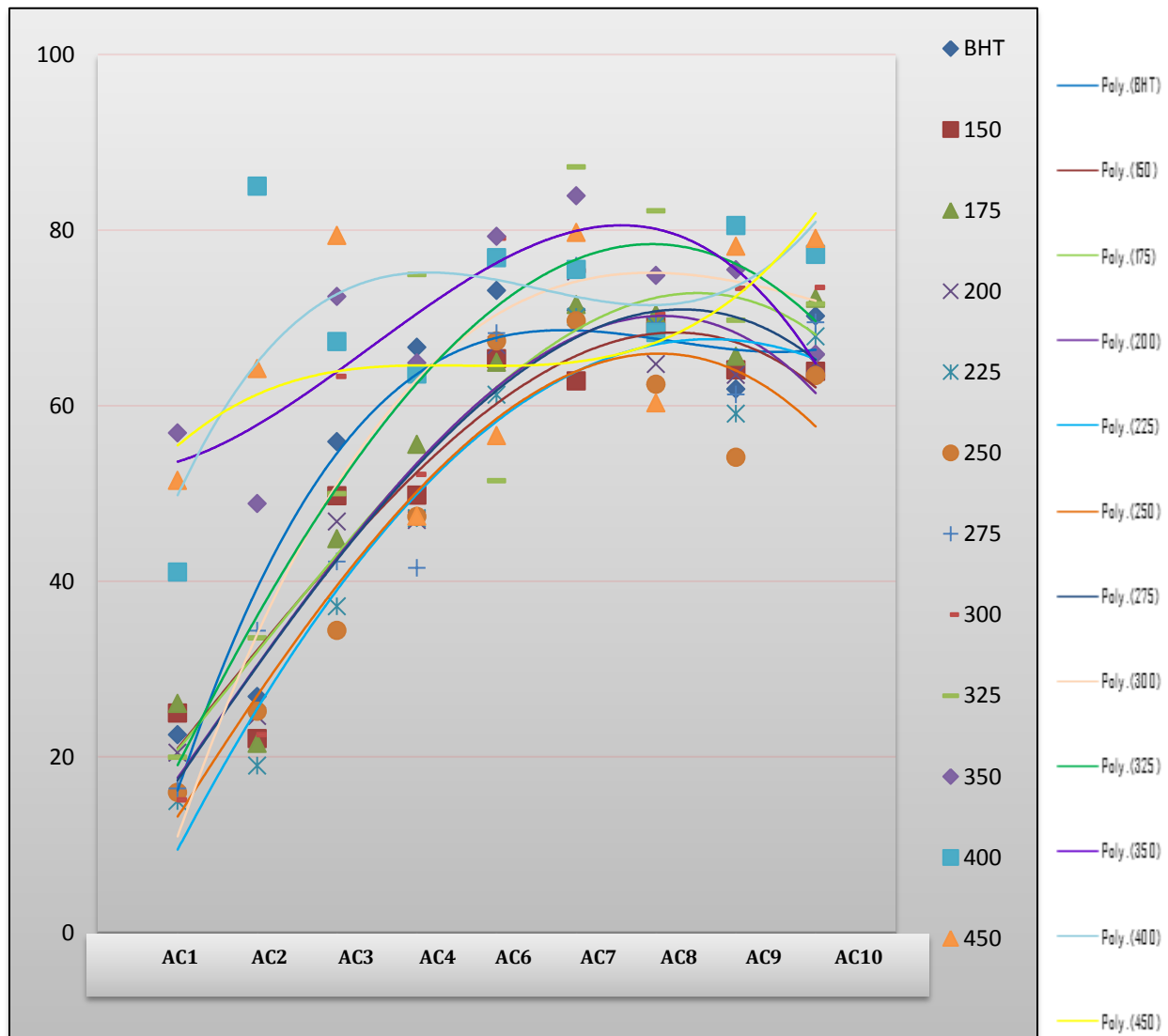


**Figure-25 Number fraction of HAGB with ARB cycles at different annealing temperature. Plots are polynomial fitted of the order 3.**



### **Texture evolution during annealing from 150 °C to 450 °C in ARB-1 to ARB-10 specimens**

In all the annealed AC-1 to AC-10 specimens with varying microstructure, the C layer mostly consisted of Cube texture components through coarsening of earlier existed ARB recrystallized grains. Whereas, in the A layer the initial ARB produced dynamical continuous recrystallized Copper and S texture grains become recovered and started coarsening with increase in annealing temperature. A layer also started generating Cube texture grains at higher temperature annealing through static discontinuous recrystallization.

But with annealing of high ARB cycle specimens when the C layer grains started consuming the A layer grains, the microstructure became cellular with mostly Cube texture grains from C layer and few remnant Copper and S texture grains of A layer.

The final microstructure of low ARB cycle specimen annealed at 450 °C contained layered microstructure with mostly Cube texture of large grains in C layer and small coarse grains in A layer. Whereas, 450 °C annealed higher ARB cycle specimens produced equiaxed coarse grains of Cube texture.

Overall higher temperature varied microstructure mainly contained Cube texture appeared through recrystallization and grain growth.

# Chapter 6

## Summary

(A) Ultra pure aluminium (99.999 wt%, C) and commercially pure aluminium (99.5 wt%, A) sheets are accumulative roll bonded in one (AC-1) to ten cycles (AC-10). From ARB-1 to AC-6, the A layer was first heavily deformed and then continuous recrystallized and the pure C layer was under discontinuous recrystallization, mainly generating grains with HAGB. From 7 cycles (AC-7) onwards, fragmentation of pure C layer grains started taking place with consumption of A layer grains. By AC-10, a fully developed ultra-fine grains with HAGB is obtained. The evolution of rolled microstructure from ARB-1 to ARB-10 is schematically shown below.

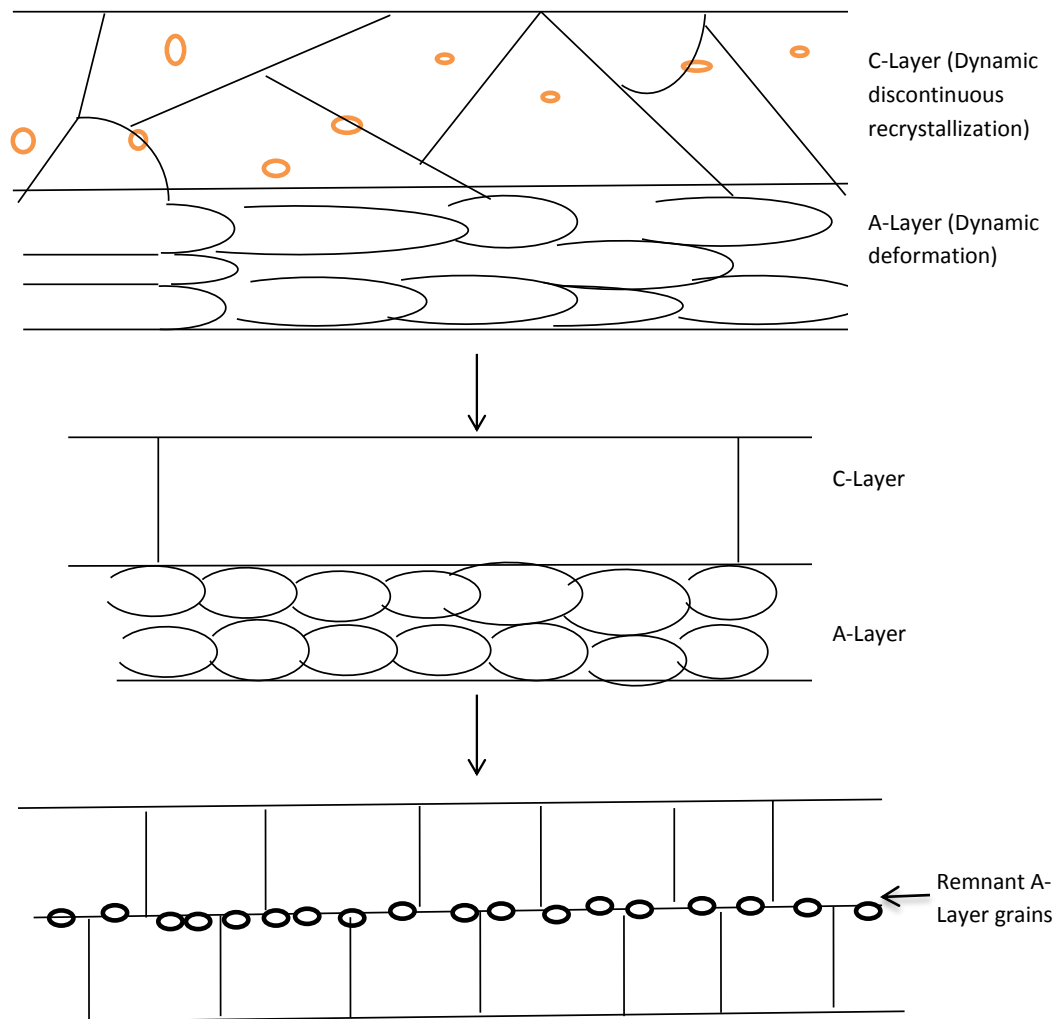
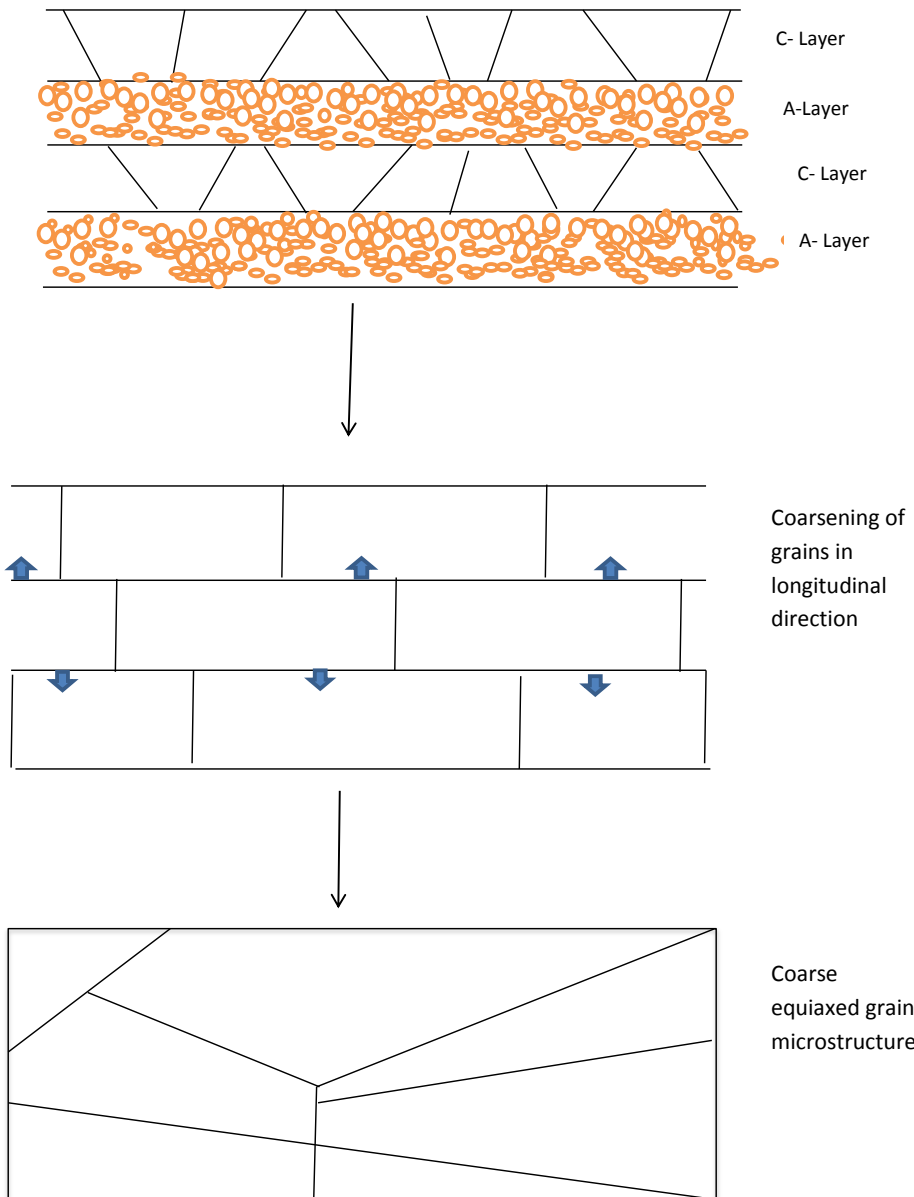


Figure-26 Schematic diagram of microstructure evolution from AC-1 to AC-10.

(B) In ARB specimens (AC-1 to AC-10) Cube and shear Cube texture components are majorly noted in C layer with Copper, S, Shear Copper and Shear S are found in A layer. The shear components might be generated from the friction between the rolls and the specimen surface.

(C) Annealing from 150 °C to 450 °C of AC-1 to AC-10 specimens produced microstructure variations from ultrafine grained ARB microstructure into coarse long cellular-type microstructure and then coarsened into large equiaxed microstructure. These microstructure variations mainly occurred under static recrystallization and grain coarsening. The microstructure variation from annealing is shown below.



**Figure-27 Schematic diagram of microstructure evolution during annealing of specimens of AC-1 to AC-10.**

(D) Annealing of all the ARB specimens (AC-1 to AC-10) generated mostly Cube texture grains.

# Chapter 7

## Future Works

- Calculation of Recrystallized volume fraction of grains from EBSD maps.
- In depth analysis of pole figures and ODF maps for micro texture evolution of annealed samples and compare the texture results with hardness data.
- Due to heterogeneous grains in the laminates of different purity aluminium laminates, there is need to calculate grain size of each layer separately.

# References

- [1] Erb, U. (1995). Electrodeposited Nanocrystals - Synthesis, Structure, Properties and Future Applications, *Canadian Metallurgical Quarterly*, 34, 275-280.
- [2] Gleiter, H. (1989). *Progress in Materials Science*, 33, 223.
- [3] W.Cao, Synthesis of Nanomaterials by High Energy Ball Milling. Skyspring Nanomaterials, Inc.
- [4] Suryanarayana, C. (1999). Non-equilibrium processing of materials, Pergamon Press.
- [5] Chen, I. W. and Wang, X. H. (2000). Sintering dense nanocrystalline ceramics without final-stage grain growth, *Nature*, 404, 168-171.
- [6] Shaw, L. L. (2000). Processing nanostructured materials: An overview, *JOM-Journal of the Minerals Metals and Materials Society*, 52, 41-45.
- [7] Valiev, R. Z., Islamgaliev, R. K. and Alexandrov, I. V. (2000a). Bulk nanostructured materials from severe plastic deformation, *Progress in Materials Science*, 45, 103-189.
- [8] Viswanathan, V., Laha, T., Balani, K., Agarwal, A. and Seal, S. (2006). Challenges and advances in nanocomposite processing techniques, *Materials Science and Engineering R*, 54, 121-285.
- [9] R.Z. Valiev, T.G. Langdon, *Prog. Mater. Sci.* 51 (2006) 881–981.
- [10] R.Z. Valiev, R.K. Islamgaliev, I.V. Alexandrov, *Prog. Mater. Sci.* 45 (2000) 103 -189
- [11] G. Sakai, Z. Horita, T.G. Langdon, *Mater. Sci. Eng. A* 393 (2005) 344–351.
- [12] Y. Saito, H. Utsunomiya, N. Tsuji, T. Sakai, *Acta Mater.* 47 (1999) 579–583.
- [13] D. Terada, S. Inoue, N. Tsuji, *J. Mater. Sci.* 42 (2007) 1673–1681.
- [14] M. Shaarbafe, M.R. Toroghinejad, *Mater. Sci. Eng. A* 473 (2008) 28–33.
- [15] Y. Saito, N. Tsuji, H. Utsunomiya, T. Sakai, R.G. Hong, *Scripta Mater.* 39 (1998) 1221–1227.
- [16] Korbel A, Richert M, Richert J (1981), The Effects of Very High Cumulative Deformation on Structure and Mechanical Properties of Aluminium. Proceedings of Second RISO International Symposium on Metallurgy and Material Science, Roskilde, September 14–18, 445–450.
- [17] J. Yin, J. Lu, H. Ma, P. Zhang, *J. Mater. S*
- [18] D.H. Shin, J.-J. Park, Y.-S. Kim, K.-T. Park, *Mater. Sci. Eng. A* 328 (2002) 98–103. *sci.* 39 (2004) 2851–2854.

- [19] Nakamura K, Neishi K, Kaneko K, Nakagaki M, Horita Z (2004) Development of Severe Torsion Straining Process for Rapid Continuous Grain Refinement. *Materials Transactions* 45(12):3338–3342
- [20] Michael J. Zehetbauer, Ruslan Z Valiev Nanomaterials by severe plastic deformation
- [21] Y. Saito, N. Tsuji, H. Utsunomiya, T. Sakai, R. G. Hong: Ultra-fine grained bulk aluminium produced by accumulative roll-bonding (ARB) process, *Scripta Materialia* 39, No.9 (1998) 1221-1227
- [22] N. Tsuji, Y. Saito, S. H. Lee, Y. Minamino: ARB and other new techniques to produce bulk UFG materials, *Advanced Engineering Materials* 5 (2003) 338-344
- [23] Tsuji, N., Saito, Y., Ito, Y., Utsunomiya, H. and Sakai, T. (2000). Ultrafine grained ferrous and aluminium alloys produced by accumulative roll-bonding, *JOM, The minerals, metals and Materials Society*, 218.
- [24] Tsuji, N., Ito, Y., Saito, Y. and Minamino, Y. (2002a). Strength and ductility of ultrafine grained aluminium and iron produced by ARB and annealing, *Scripta Materialia*, 47, 893-899.
- [25] Xing, Z. P., Kang, S. B. and Kim, H. W. (2002). Structure and properties of AA3003 alloy produced by accumulative roll bonding process, *Journal of Materials Science*, 37, 717-722.
- [26] Ohsaki, S., Kato, S., Tsuji, N., Ohkubo, T. and Hono, K. (2007). Bulk mechanical alloying of Cu-Ag and Cu/Zr two-phase microstructures by accumulative rollbonding process, *Acta Materialia*, 55, 2885-2895.
- [27] Jiang, L., Ruano, O. A., Kassner, M. E. and Perez-Prado, M. T. (2007). The fabrication of bulk ultrafine-grained zirconium by accumulative roll bonding, *JOM Journal of the Minerals, Metals and Materials Society*, 59, 42-45.
- [28] Kamikawa, N., Tsuji, N. and Saito, Y. (2003). Effect of strain on microstructures and mechanical properties of ARB processed and annealed ultra-low carbon IF steel, *Tetsu to Hagane-Journal of the Iron and Steel Institute of Japan*, 89, 63-70.
- [29] Tsuji, N., Ueji, R. and Minamino, Y. (2002b). Nanoscale crystallographic analysis of ultrafine grained IF steel fabricated by ARB process, *Scripta Materialia*, 47, 69-76.
- [30] Koizumi, Y., Ueyama, M., Tsuji, N., Minamino, Y. and Ota, K. (2005). Internal friction of ultrafine-grained nickel produced by Accumulative Roll-Bonding (ARB), *Journal of the Japan Institute of Metals*, 69, 997-1003.
- [31] Tsuji, N., Kato, S., Ohsaki, S., Hono, K. and Minamino, Y. (2005). Bulk mechanical alloying of Zr-Cu system by accumulative roll bonding (ARB), *Metastable, Mechanically Alloyed and Nanocrystalline Materials*, 24-25, 643-646, 742.

- [32] Eizadjou, M., Talachi, A. K., Manesh, H. D., Shahabi, H. S. and Janghorban, K. (2008). Investigation of structure and mechanical properties of multi-layered Al/Cu composite produced by accumulative roll bonding (ARB). *Process, Composites Science and Technology*, 68, 2003-2009.
- [33] Sakai, T., Saito, Y., Kanzaki, T., Tamaki, N. and Tsuji, N. (2001). Grain Refinement of Cu-Co-P Alloy by Accumulative Roll Bonding, *Journal of the Japan Copper and Brass Research Association*, 40, 213-217.
- [34] Chowdhury, S. G., Dutta, A., Ravikumar, B. and Kumar, A. (2006a). Textural evolution during accumulative roll bonding of an Al-Li alloy, *Materials Science and Engineering a-Structural Materials Properties Microstructure and Processing*, 428, 351-357.
- [35] Humphreys, F. J. and Hatherly, M. (2004). *Recrystallization and Related Annealing Phenomena*, Oxford, UK, Elsevier.
- [36] J.W. Hutchinson. *Proc R Soc London A* 319 (1970) p. 247.
- [37] J.R. Kissell, R.L. Ferry. *Aluminium structures: a guide to their specifications and design*, second ed. New York: John Wiley&Sons;2002
- [38] Hansen, N. (2001). Microstructural evolution during forming of metals, *Journal of Materials Science and Technology*, 17, 409-412.
- [39] D. A. Hughes, N. Hansen: High angle boundaries formed by grain subdivision mechanism, *Acta Materialia* 45 (1997) 3871-3886
- [40] Liu, Q., Juul Jensen, D. & Hansen, N. 1998 Effect of grain orientation on deformation structure in cold-rolled polycrystalline aluminium. *Acta Mater.* 46, 5819-5838.
- [41] F. J. Humphreys, M. Hatherly: *Recrystallization and related annealing aluminium phenomena*, Oxford: Pergamon Press, 1995
- [42] G. Gottstein: *Physikalische Grundlagen der Materialkunde*, Springer Verlag Berlin Heidelberg 1998
- [43] J.W. Evancho, J.G. Kaufman, *Aluminum* 53 (1977) 609.
- [44] D.G. Altenpohl, *Aluminum, Technology, Applications, and Environment, A Profile of a Modern Metal*, Sixth Edition, TMS, 1998, pp. 360–364.
- [45] L.P. Troeger, E.A. Starke Jr, *Mater. Sci. Eng. A277* (2000) 102.
- [46] D. Marchive, *Light Metal Age* 41 (1983) 6.
- [47] M. Merklein: *Charakterisierung von Blechwerkstoffen für den Leichtbau*, Maisenbach Verlag 2006, Bamberg
- [48] Audi AG, [www.audi.de](http://www.audi.de), 2008
- [49] N.Tsuji, Y.Ito, Y.Saito and Y.Minamino: *Scr.mater.* 47(2002)893-899.



- [50] N.Tsuzi, X.Huang and H.Nakashima:Proc. Of 25th Riso Int.Symp. on Mater. Sci.:Evolutio of Deformation Microstructures in 3D, (Riso National Laboratory, Roskilde, Denmark, 2004) pp. 147-170.
- [51] Thermomechanical processing of metallic materials by Bert Verlinden, Julian Driver, Indradev Samajdar and Roger D. Doherty
- [52] Humphreys, F. J. & Hatherly, M. 2004. Recrystallization and related annealing phenomena. 2nd edn. Oxford, UK: Pergamon.
- [53] [www.asminternational.org](http://www.asminternational.org) “grinding and polishing” Ceramography: Preparation and Analysis of Ceramic Microstructures (#06958G).
- [54] H.W. Kim, S.B. Kang, N. Tsuji, Y. Minamino, Metall. Mater. Trans. A 36 (2005) 3151–3163.
- [55] English A. T. and Chin G. Y., Acta Metall., 13 (1965) 1013.
- [56] Lucke K., Proc. Sixth Int. Conf. Text. Mater. 1(1981) 14.
- [57] Materials Science and Engineering: A, Volume 391, Issues 1–2, 25 January 2005, Pages-377-389 A.P. Zhilyaev, B.-K. Kim, J.A. Szpunar, M.D. Baró, T.G. Langdon.
- [58] Introduction to texture analysis: macro texture, micro texture, and orientation mapping / Olaf Engler and Valerie Randle.
- [59] Paul Chekhonin, Benoît Beausir, Juliane Scharnweber: Acta Materialia 60 (2012) 4661–4671.

# Appendix I

## 1.1 Solid solution strengthening

Highly pure metals can be strengthened by addition of alloying elements. If the size of alloying atoms and solvent matrix atoms is same, some of the solvent atoms are substituted by alloying atoms, therefore it is called as substitutional solid solution and if the alloying atoms are of very smaller size compared to the solvent matrix they occupy interstitial positions in the matrix, therefore it is called as interstitial solid solution. Both the solid solutions are strengthened due to the presence of alloying atoms, which resist the mobility of dislocation thereby increasing the stress required for plastic flow. Solute atoms can interact with dislocations by some possible ways such as, Praelastic, dielectric and chemical interaction.

In case of paraelastic interaction there is atomic size difference between alloying atoms and solvent matrix, this causes lattice strains on surrounding host atoms. Due to lattice strain field interaction between the dislocations and alloying atoms, dislocation movement restricted. Thus, to overcome this resistance and to initiate and continue plastic deformation greater stress must be applied. Dielectric interaction is based on the fact that alloying elements have a different shear modulus than the solvent matrix atoms, therefore increases the resistance to dislocation motion. In the case of chemical interaction, there is a dragging force, which creates hindrance for dislocation motion.

## 1.2 Precipitation Hardening

Precipitation hardening can be achieved by solutionising, quenching and annealing of the alloy. Precipitate particles in a matrix provide obstacles for the dislocation motion. Thus for dislocation motion through the matrix phase there is two way either they cut through the precipitate particles or bend around and bypass them. First one is possible if the slip plane is continuous from the matrix through the precipitate particles and when the stress to dislocation movement through the precipitate particle is comparable to that in the matrix. Bending around the precipitate particles is possible if there is interspacing between precipitate particle and matrix and abrupt misorientation at the interface. The stress required to bend a dislocation is inversely proportional to the average inter-particle spacing. Thus, effective strengthening can be achieved in the bending process, if the precipitate particles are submicroscopic sizes.

## 1.3 Strain (work or dislocation) hardening

The principal of strain hardening is dislocation generation, dislocation motion and dislocation interaction. During strain hardening the dislocation source (Frank-Reed source) becomes activated and number of dislocations increases. Since, dislocations incorporates strain field which interact with each other and making difficult for the next dislocation to move further through the strain field.

## 1.4 Grain boundary strengthening

Well known equation of Hall-Petch suggests that, with decreasing the size of grains yield strength increases. Dislocations are piled-up at the grain boundaries and for further mobility of dislocations additional stress requires. Therefore, grain boundaries become efficient barrier to dislocation movement.

## 2 Annealing effects (reliving of stored energy)

Ultra-fine grained materials have a high stored energy ( $J/m^3$ ), which provides driving force for recovery and recrystallization. Therefore, ultra-fine grained metals have a poor thermal stability. It has also been found that the ARB processed materials shows limited ductility, normally it is 10% of the total elongation in uniaxial tension [49-50]. Thus to make this processed material enough ductile annealing after deformation is required. At low temperature ( $0.4-0.5 T_m$ ) recovery dominates and often results in slow decrease in hardness. At high temperature ( $0.7T_m$ ) recovery occurs very rapidly without much prior recovery [51]. During deformation high energy is accumulated in the material and during annealing this energy released. Therefore, in order to optimize properties of ultra-fine grained materials, studies on the effect of heat treatments on the structure and properties of nanostructured metals are of great importance. The main material factors that affect static annealing include chemical composition, initial grain size, microstructure, texture, second phase particles and solute distribution and some processing parameters are deformation mode, strain, strain rate and temperature [52]. The restoration processes are conventionally classified into three categories: recovery, recrystallization and grain growth [52].

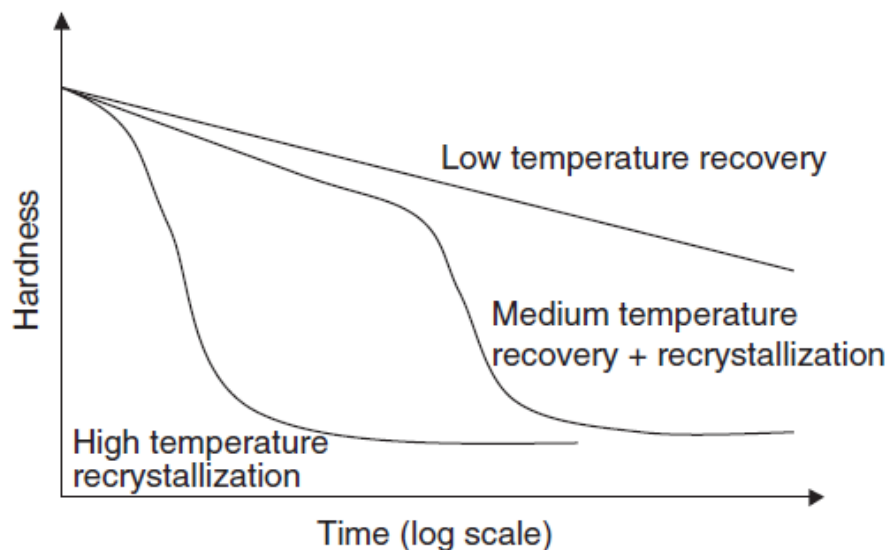


**Figure 1: Schematic diagram representing the softening kinetics by recovery and recrystallization at various temperatures [51].**

## 2.1 Recovery

During recovery, some of the stored internal energy is relieved and physical properties of the material before plastic deformation restored without any significant change in microstructure. Various mechanisms of recovery involves annihilation of closely spaced dislocations of opposite sign or dipoles, organization of free, random dislocations into dislocation walls or sub-boundaries and coalescence of sub-boundary walls during sub-grain growth. These mechanisms are shown in figure:

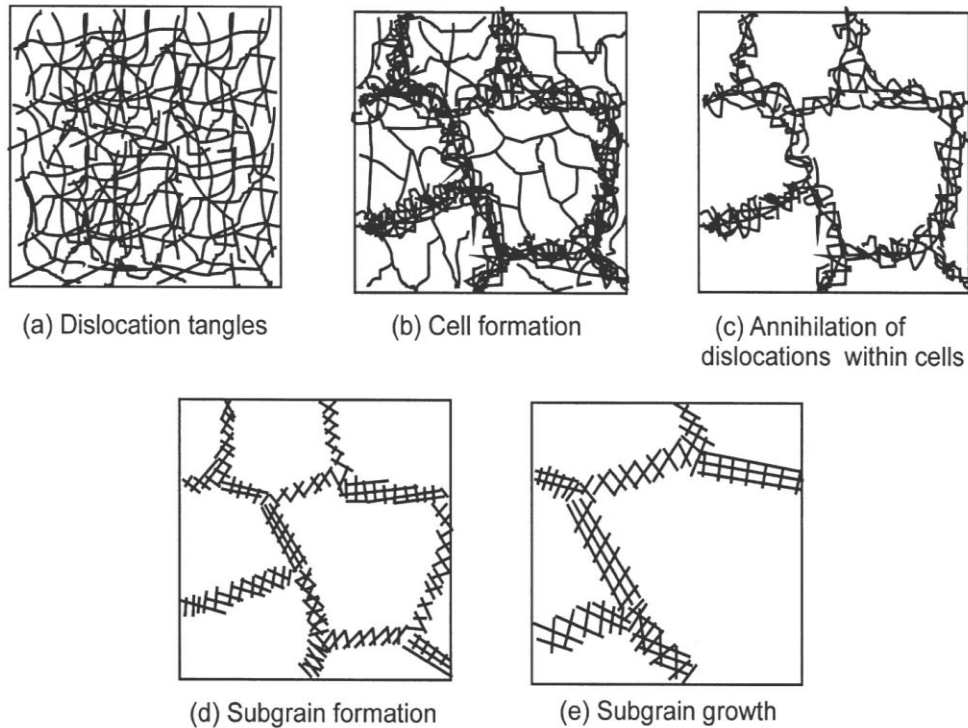


**Figure 2: Schematic recovery process representing various steps of recovery during annealing after deformation [52].**

It is found that solute atoms play an important role in recovery kinetics. For example, deformed ultrahigh pure metals can recover at about  $0.2T_m$  and start recrystallization at  $0.3T_m$  but in presence of solute atoms the recovery and recrystallization temperature push up to  $0.4T_m$  to  $0.6T_m$ , respectively [51]. Through recovery, the strength is slightly decreased but the ductility significantly increases.

## 2.2 Recrystallization and grain growth

Recrystallization is the formation of new set of strain free grains in deformed material. Recrystallization occurs by the formation and migration of high angle boundaries, while grain growth is subsequently grow and consume the recovering substructure. The driving force for recovery and recrystallization is stored energy of deformation, whereas the driving force for grain growth is decrease in surface area.

The process of nucleation originates from the cells or sub-grains developed by the deformation, and the nuclei being highly misoriented with the surrounding cells or sub-grains.

For growth of the nuclei, it must be greater than a critical radius,  $R_c$ . the relation between critical radius and grain boundary energy  $\gamma$  and stored energy is  $E$  is:

$$R_c = 4E / \gamma$$

The following table shows continuous and discontinuous recovery and recrystallization and grain growth (static annealing phenomena).

**Table 1: Summary of static annealing phenomena [41].**

<b>Restoration Process Type</b>	<b>Recovery</b>	<b>Recrystallization</b>	<b>Grain Growth</b>
<b>Continuous</b>	Subgrain growth	Continuous recrystallization	Normal grain growth
<b>Discontinuous</b>	Discontinuous subgrain growth	Primary recrystallization	Abnormal grain growth

In the figure the continuous and discontinuous restoration processes are defined schematically. In the continuous process recovery, recrystallization and normal grain growth occurs and microstructure coarsen gradually with no major nucleation event. While in discontinuous process abnormal grain growth occurs and involves nucleation and preferential growth of certain grains throughout the microstructure.

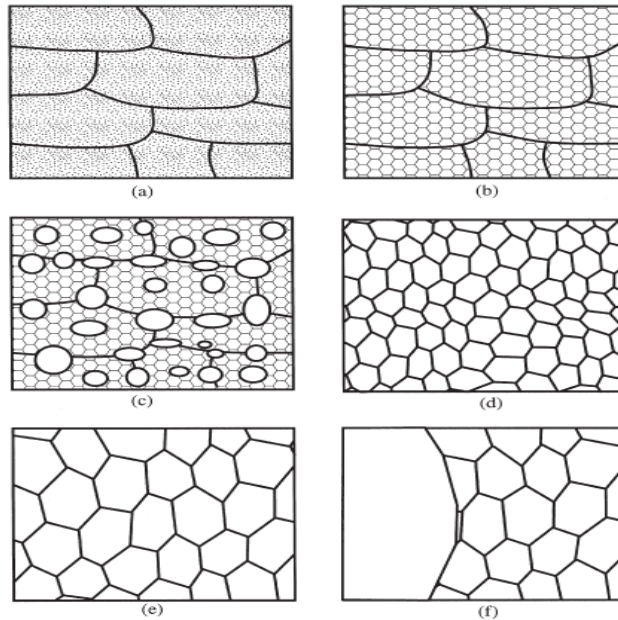


**Figure 3: Schematic diagram of main annealing processes (a) deformed state, (b) recovered, (c) partially recrystallized, (d) fully recrystallized, (e) grain growth and (f) abnormal grain growth [52].**

### 2.3 Dynamic recovery and Recrystallization

Sometimes restoration processes may occur during deformation at high temperatures which give rise to dynamic recovery and recrystallization. However, very pure metals can be recrystallized during cold deformation process itself.

For metals with high stacking fault energy, dislocation climb and cross slip occur very easily, thus at high temperatures dynamic recovery is rapid and extensive. In this case flow stress saturates after an initial period of work hardening.

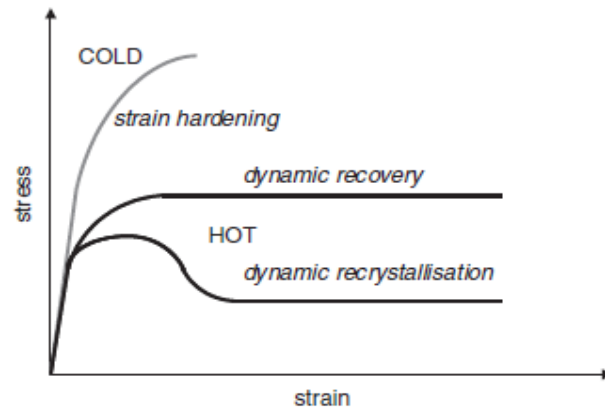


**Figure 4: Flow curves (stress vs. strain) during cold and hot deformation [51].**

During dynamic recovery the original grains highly strained but sub-boundaries remains equiaxed. Whereas in low or medium SFE materials recovery process is slow and at critical strain dynamically recrystallized grains appears at the original grain boundaries. With increase in strain more nuclei activate and recrystallized grains appear. Simultaneously the recrystallized grains in previous stage deformed again. After a certain amount of strain due to dislocation accumulation and dynamic recrystallization saturation or equilibrium reached. At this stage, the flow curve reaches a plateau and the microstructure consist of a dynamic mixture of grains with various dislocation densities.

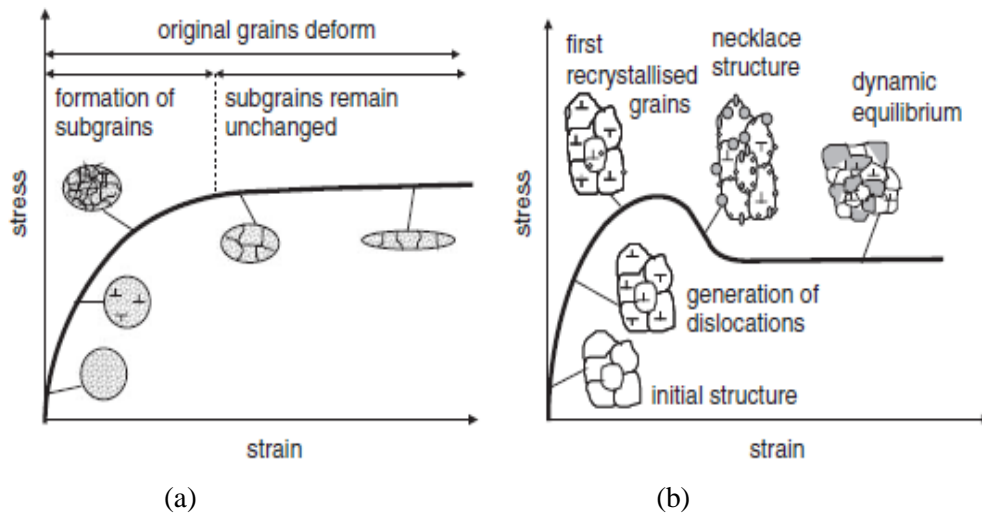


**Figure 5: microstructure evolution during (a) hot deformation of a metal showing recovery and (b) dynamic recrystallization [51].**

Kassner and Evangelista (1995) concluded that discontinuous recrystallization can occur during room temperature deformation of very high purity aluminium.